GSI

GSI-Preprint-97-23
April 1997



# STUDY OF THE β-DECAYS OF $^{37}$Ca AND $^{36}$Ca

W. Trinder, E.G. Adelberger, B.A. Brown, Z. Janas, H. Keller, K. Krumbholz, V. Kunze, P. Magnus, F. Meissner, A. Piechaczek, M. Pfützner, E. Roeckl, K. Rykaczewski, W.-D. Schmidt-Ott, M. Weber



( To be published in Nucl. Phys.A )

Gesellschaft für Schwerionenforschung mbH
Planckstraße 1 • D-64291 Darmstadt • Germany
Postfach 11 05 52 • D-64220 Darmstadt • Germany

# Study of the $\beta$–Decays of $^{37}$Ca and $^{36}$Ca

W. Trinder[a)*], E.G. Adelberger[b)], B.A. Brown[c)], Z. Janas[a)], H. Keller[a)], K. Krumbholz[d)], V. Kunze[d)], P. Magnus[b)], F. Meissner[d)], A. Piechaczek[a)], M. Pfützner[e)], E. Roeckl[a)], K. Rykaczewski[e)], W.-D. Schmidt-Ott[d)], M. Weber[a)]

[a)] *GSI, Darmstadt, Germany,* [b)] *Dept. of Physics, Univ. of Washington, Seattle, USA,* [c)] *Michigan State University, East Lansing, USA,* [d)] *II. Phys. Inst., Univ. Göttingen, Germany,* [e)] *Inst. of Exp. Physics, Univ. of Warsaw, Poland*

## Abstract

The $\beta$-delayed proton and $\gamma$-ray emission of $^{37}$Ca and $^{36}$Ca was studied at the projectile fragment separator at GSI Darmstadt. In the $^{37}$Ca study, the $\beta$-delayed $\gamma$-decay was observed for the first time, and the half-life was redetermined, under essentially background-free conditions, as 181.1 $\pm$ 1.0 ms. The surprisingly high $\Gamma_\gamma/\Gamma_p$ values found for proton-unbound states in $^{37}$K drastically reduce former discrepancies between the Gamow-Teller strength values $B$(GT) measured in the $^{37}$Ca $\beta$-decay and those deduced from the $^{37}$Cl(p,n)$^{37}$Ar mirror reaction. Our data provide evidence, on a level of 1.6 standard deviations, for isospin-mixing of the lowest $T = 3/2$ level in $^{37}$K. In the $^{36}$Ca study, a complete $\beta$-decay scheme, including the $\beta$-delayed proton emission into the ground and first excited states of $^{35}$Ar as well as the $\beta$-delayed $\gamma$-decay, was measured for the first time. The $^{36}$Ca half-life was remeasured with improved accuracy to be 102 $\pm$ 2 ms. Our data exclude a $1^+$ assignment for two near-threshold states in $^{36}$K that could be important resonances in $^{35}$Ar(p,$\gamma$) reactions of astrophysical interest. The $B$(GT) distributions in $^{37,36}$Ca decays are compared to results obtained from large-scale *sd* shell-model calculations.

**PACS:** 23.40.–s, 29.30.Fq, 29.30.Bk, 29.30.Kv, 23.20.Ck, 29.40.Pe, 21.60.Cs

**Keywords:** RADIOACTIVITY $^{37,36}$Ca from $^{9}$Be($^{40}$Ca,X), E = 300 A$\times$MeV; Measured $E_p$, $I_p$, $E_\gamma$, $I_\gamma$, $\beta\gamma$-, $\beta\gamma$p-coincidences; $T_{1/2}$; Ge and Si detectors; *sd*-shell model.

*Present address: GANIL, B.P.5027, 14076 Caen Cedex 5, France

# 1 Introduction

The Gamow-Teller (GT) transition strength $B$(GT) that determines part of the decay rate in nuclear $\beta$-decay is generally found to be significantly overestimated by shell-model predictions. For example, the $B$(GT) values obtained from $(2s1d)^n$ shell-model wavefunctions are in much better agreement with the experimental data if the "free-nucleon" GT operator is scaled by a factor of approximately 0.7 ("effective" operator) [1]. This effect, commonly referred to as the "quenching" of the GT strength, is ascribed mainly to two rather different effects that are omitted in conventional shell-model calculations – higher-order configurations neglected in the limited model space and subnucleonic degrees of freedom [2]. To make a decisive test of the quenching mechanism, one needs to find where the "missing strength" is located.

During the last few years improvements in experimental techniques have permitted detailed studies of the $\beta$-decays of very proton-rich nuclei [3]. Characterized by high energy releases, these decays reveal the GT strength function for transitions covering a large range of excitation energies in the daughter nuclei. They therefore provide opportunities for stringent tests of shell-model calculations. The proton-rich side of the nuclear chart, as exemplified by $^{37}$Ca and $^{36}$Ca decays, is better suited for such studies than is the neutron-rich side, because high-resolution work is easier when the delayed heavy particles are protons and alphas rather than neutrons.

The decays of $^{37}$Ca ($Q_{EC}$ = 11639(22) keV [4]) and $^{36}$Ca ($Q_{EC}$ = 10990(40) keV [4]) also provide opportunities to compare, over a very wide range of excitation energies, $\beta$-decay $B$(GT) strengths to the corresponding $B$(GT) distributions extracted from forward-angle (p,n) reactions on the N = 20 mirror nuclei. Under the assumption of isospin symmetry, the $B$(GT) distribution for $^{37}$Ca $\beta$-decay and that inferred from $^{37}$Cl(p,n)$^{37}$Ar should be identical, as should those extracted from $^{36}$Ca $\beta$-decay and inferred from $^{36}$S(p,n)$^{36}$Cl. The A = 37 $B$(GT) function is also of astrophysical interest since it determines the neutrino-capture rate of $^{37}$Cl. This cross-section is needed for calibrating the solar-neutrino flux by measured by the $^{37}$Cl detector [5]. Finally, the study of the $\beta$-decay of $^{36}$Ca can give information about the properties of near-threshold states in $^{36}$K that could be resonances in the astrophysically important $^{35}$Ar(p,$\gamma$)$^{36}$K reaction.

A previous high-resolution study of the $\beta$-delayed proton emission of $^{37}$Ca [6] gave $B$(GT) values that differed significantly from those extracted in a $^{37}$Cl(p,n)$^{37}$Ar study [7]. These discrepancies were too large to be ascribed to isospin asymmetries alone [8]. A subsequent $^{37}$Cl(p,n) study with higher resolution and polarization transfer information [9] reduced part of the discrepancy by finding additional GT strength in the vicinity of the analog transition. Later, investigations of the $^{40}$Ca(p,$\alpha$)$^{37}$K [10] and $^{36}$Ar(p,$\gamma$)$^{37}$K [11] reactions showed that some proton-unbound

states in $^{37}$K have significant probabilities for decaying via $\gamma$-ray emission. Therefore part of the $B$(GT) asymmetries claimed for the A = 37 system might have originated from an incorrect assumption [6] - that all proton-unbound daughter states in $^{37}$Ca $\beta$-decay had $\Gamma = \Gamma_p$. In the case of $^{36}$Ca, a previous study of its $\beta$-decay [12] yielded only an estimate of 100 ms for the half-life and a value of 4258(24) keV for the excitation energy of the isobaric analog state (IAS) in $^{36}$K that was remeasured recently to be 4289(8) keV [13].

In order to clarify the discrepancies between the A = 37 GT strengths determined by previous experiments and to shed more light on the quenching of GT strength, we reinvestigated the decay of $^{37,36}$Ca, observing both the $\beta$-delayed proton emission ($\beta$p) into the ground and excited states of $^{36,35}$Ar as well as the $\beta$-delayed $\gamma$-decay ($\beta\gamma$) of $^{37,36}$Ca.

After a description of the experimental techniques in the next section, the experimental data will be presented in Section 3. Section 4 contains the discussion of the results, including a comparison of the measured $B$(GT) functions with recent shell-model calculations, summary and outlook are given in Section 5. Preliminary results of this work have already been given in [14, 15] while part of the final data was presented briefly in [16]-[20]. This report gives a more detailed description of the experimental procedures as well as of the physics aspects.

## 2 Experimental techniques

The experiment used the projectile fragment separator FRS [21] at GSI Darmstadt. Secondary beams of $^{37}$Ca and $^{36}$Ca were produced in separate experiments by fragmentation reactions of a 300 A$\times$MeV $^{40}$Ca beam impinging on a 1g/cm$^2$ $^{9}$Be target. A shaped aluminum degrader mounted in the intermediate focal plane of the FRS improved the B$\rho$ selection of the four dipoles [22] (see Figure 1a). The isotopes transmitted to the final focus of the FRS and implanted into a silicon counter were identified by their energy loss ($\Delta$E) and time-of-flight (TOF) [23]. The TOF signal was obtained from two scintillation detectors mounted at the intermediate and final foci of the FRS while the $\Delta$E signal was measured in a MUSIC detector (MUlti-Sampling Ionisation Chamber) [24] positioned at the final focus. This location also contained two MWPC detectors (Multi-Wire Proportional Chamber) [25] that gave the implantation profile perpendicular to the beam direction [26], slits in front of the spectroscopy setup, and various aluminum degraders that allowed us to shift the implantion depth of the nuclei inside the silicon detectors (see Figure 1b).

In two subsequent settings of the FRS, beams of about 30 $^{37}$Ca atoms/s and 1 $^{36}$Ca atom/4s were implanted into a 30 mm $\times$ 30 mm $\times$ 500 $\mu$m silicon counter (implantation detector). This detector was positioned between two silicon counters of similar dimensions for detecting $\beta$-rays

($\beta$-detectors), while two large-volume germanium detectors registered $\gamma$-rays emitted by the implanted nuclei (see Figure 1c).

The aluminum degrader was adjusted to give a very narrow $^{37,36}$Ca implantation profile along the beam direction (FWHM $\approx$ 100 $\mu$m, see Figure 2) that was centered around an implantation depth of 250 $\mu$m. This assured that protons with energies up to about 4 MeV were fully stopped in the implantation detector, while higher-energy protons deposited sufficient energy to produce clear lines in the $^{36}$Ca $\beta$p spectrum. The narrow profile allowed us to trigger with essentially 100% efficiency on events where $\gamma$-rays were emitted by the implanted activity; this was done using the energy loss of the coincident $\beta$-rays recorded in the implantation detector. Hence, only $\gamma$-rays originating from nuclei decaying inside the implantation detector were measured and the room background was suppressed efficiently.

The FRS setting for the $^{37}$Ca experiment gave a secondary beam at the final focus containing 82.3% $^{37}$Ca along with the isotonic contaminants $^{36}$K (16.4%) and $^{35}$Ar (1.3%). A similar beam composition was obtained for the tuning on $^{36}$Ca, the impurities being $^{35}$K and $^{34}$Ar in that case. The $\Delta$E signal of the MUSIC chamber was sufficient to identify the isotopes implanted into the implantation detector as shown for the setting on $^{37}$Ca in Figure 3.

The numbers of implanted $^{37,36}$Ca atoms N($^{37,36}$Ca), needed for normalizing the decay rates, were determined by two independent methods: (i) from the number of identified $^{37,36}$Ca atoms corrected for losses due to secondary reactions in the stopping process (11(1)% for $^{37}$Ca, 11(2)% for $^{36}$Ca [26, 27]), and (ii) by counting all subsequent $^{37,36}$Ca positron-decay events. The second method, which will be explained here for the case of $^{37}$Ca, is based on the fact that each decay of $^{37}$Ca, its daughter $^{37}$K, and the implanted contaminants $^{36}$K and $^{35}$Ar is accompanied by the emission of a positron and partially also a proton. It is thus possible to obtain the number of $^{37}$Ca atoms, that disintegrated in the implantation detector, from the total number of decay events measured in this detector. This evaluation makes use of the *relative* intensities of implanted $^{37}$Ca, $^{36}$K and $^{35}$Ar atoms, obtained from the MUSIC spectrum (Figure 3), and implies the following assumptions:

- The $\beta$p decay of $^{37}$Ca leads to the stable isotope $^{36}$Ar while all other $^{37}$Ca decay events are followed by a subsequent $^{37}$K $\beta$-decay.
- $^{37}$Ar, the daughter of $^{37}$K, is not considered because of its pure electron-capture decay ($Q_{EC}$ = 813.5(3) keV [4]).
- Electron-capture contributions are negligible for the $\beta$-decays of $^{37}$Ca, $^{36}$K and $^{35}$Ar, which are either dominated by positron emission due to Q-value arguments [28] or followed by

charge-particle emission.

- $\beta$-decay of secondary reaction products is neglected since they are stopped well downstream of the implantation detector (for details see [26]).

The two values determined by method (i) and (ii) for N($^{37}$Ca) agree to better than 1%. The same is true for N($^{36}$Ca). The total numbers of atoms implanted in our experiment were 2.6 $\times$ $10^6$ and 2.8 $\times$ $10^4$ for $^{37}$Ca and $^{36}$Ca, respectively.

The energy resolution of the $\beta$p spectrum in the implantation detector was very poor because the continuously distributed energy loss of the coincident $\beta$-ray was added to each proton signal. Therefore, the $\beta$p energy calibration and the $\beta$p decay intensities for $^{37}$Ca were determined by comparing the $\beta$p spectrum from this work with the high-resolution data [6]. The $\beta$p energy calibration in the $^{36}$Ca measurement was based on $\alpha$-calibration sources and the $\beta$p spectrum of the $^{37}$Ca experiment. The latter procedure took advantage of the fact that the $^{37}$Ca and $^{36}$Ca $\beta$-decay energy releases (see above) and proton separation energies ($S_p(^{36}K)$ = 1666(8) keV, $S_p(^{37}K)$ = 1857.77(09) keV [4]) are similar. Because the implantation profiles were practically the same for $^{37}$Ca and $^{36}$Ca, the line shifts due to summing of the $\beta$-ray energy loss with proton energy were almost equal. Furthermore, the *difference* of the line shifts due to pulse-height defects of the recoil atoms ($^{35}$Ar, $^{36}$Ar) in the decays of $^{36}$Ca and $^{37}$Ca was negligible [29, 30].

To determine the $\beta\gamma$-decay rates, a precise calibration of the $\gamma$-efficiency was carried out using a calibrated $^{56}$Co source. The spatial distribution of this source corresponded to the implantation profile perpendicular to the beam direction deduced from the MWPC spectra during the experiment [26]. Since almost every $\gamma$-ray emitted from $^{56}$Co is part of a $\gamma$-cascade [31], a correction for cascade summing effects, which was important in our high-efficiency detection setup, was made [26]. The detection geometry also required a correction for losses in the photopeaks of $\beta\gamma$-lines due to summation with $\beta$-rays or 511 keV annilihation radiation [26]. It was found that these effects diminished the intensity of the $\gamma$-lines by 10–20%, depending on the corresponding $\beta$-endpoint energy.

For the half-life determinations, we used proton spectra accumulated in a pulsed beam-mode – 0.5s (0.2s) beam on, 2.5s beam off for $^{37}$Ca ($^{36}$Ca). The time of each decay event was recorded with a high-precision clock. Only the beam-off data were used for these measurements. To insure that the measured time spectra were free of $\beta$-ray energy loss signals from the decay of contaminants or daughter nuclei, we required a coincidence with one of the $\beta$-detectors. This reduced the $\beta$-ray energy loss (see below). This coincidence condition allowed us to trigger only on protons with energies above 3 MeV and 2.5 MeV for $^{37}$Ca and $^{36}$Ca, respectively. These originated mainly from the Fermi $\beta$-decay, and gave very clean, essentially background-free

time spectra. A time-dependent correction for dead-time effects, extracted from a randomly distributed pulser, was included in the half-life analysis for $^{37}$Ca [26]. The maximum dead-time loss, which occurred at the beginning of the beam-off period, was about 20 %. Figure 4 shows our lifetime data; the $^{37}$Ca half-life was determined to be $T_{1/2}$ = 181(1)ms, which is two standard-deviations longer than the previously accepted result [32].

# 3 Results and discussion

## 3.1 Results for $^{37}$Ca

### 3.1.1 *β-delayed γ and proton decay of $^{37}$Ca*

Figure 5 shows the $\gamma$-ray spectrum observed for $^{37}$Ca. The $\gamma$-deexcitation of the first three excited states of $^{37}$K at 1370.9(2), 2750.4(2) and 3239.3(2) keV, fed in allowed $\beta$-decay of $^{37}$Ca with $\beta\gamma$-branching ratios of 2.1(1), 2.8(1) and 4.8(2)%, respectively, was observed for the first time in our experiment. In evaluating the $\beta$-decay feeding of the 2750 keV level, we took into account the known [32] $\gamma$-deexcitation pattern of this state. The $^{36}$Ar $\gamma$-rays [32] originated mainly from the $\beta$-decay of the implanted contaminant $^{36}$K, but also from the $\beta$p decay of $^{37}$Ca into excited states of $^{36}$Ar [6]. We observed that the 3239.3 keV state was fed with a total $\beta$-decay branching ratio of 5.1(2)% corresponding to a log*ft* value of 4.85(2), which indicates an allowed transition. We therefore identify this level, previously reported as ($J^\pi = \frac{5}{2}^+, \frac{7}{2}^+$) [32], as the analog of the $J^\pi = \frac{5}{2}^+$ state at 3171.3 keV in $^{37}$Ar [32]. A subsequent experiment using NaI detectors [33], found $\beta\gamma$-decay branching ratios of 1.5(4), 3.6(8), and 4.4(6)% for the states at 1370.9, 2750.4 and 3239.3 keV, respectively.

Figure 6 shows the proton spectrum measured in the implantation detector. Spectrum a) shows the raw spectrum while spectrum b) was accumulated in coincidence with a $\beta$-ray energy-loss signal in the downstream $\beta$-detector. This condition selected short $\beta$ flight paths in the implantation detector and reduced the summing effects in the proton line shape. In spectrum c) the resolution was further improved by requiring a small $\beta$-ray energy deposit ($\Delta E_\beta \leq 450$ keV) in the downstream detector which exploited the smooth behaviour of the energy-loss characteristics of high-energy $\beta$-rays [34]. As can be clearly seen in Figure 6, the different coincidence conditions allowed us to separate proton lines that were not resolved in the raw spectrum. This technique was also used in determining the $\beta$-decay scheme of $^{36}$Ca (see below).

The $\beta$-decay scheme of $^{37}$Ca is shown in Figure 7. The reduced $\beta$-decay transition strengths

were determined using the relation

$$\left[B(\mathrm{F}) + \left(\frac{g_A}{g_V}\right)^2 B(\mathrm{GT})\right]_i = \frac{K}{f(E_i)t_i}$$

where $B(\mathrm{F})$ is the Fermi strength, $g_A/g_V = -1.262$, $K = 6127(9)$ s [35], and $E_i$, $t_i$ and $f(E_i)$ are the $\beta$-endpoint energy, the partial half-life and the phase-space factor [36], respectively, of a $\beta$-transition to the $i$th daughter level. Table 2 compares the low-energy part of our $^{37}$Ca $B(\mathrm{GT})$ distribution to previous values from $\beta$p decay [6], recent $\beta\gamma$ decay data [33] (in combination with the results from [6]), and $^{37}$Cl(p,n)$^{37}$Ar reactions [7, 9, 33]. Our $B(\mathrm{GT})$ value of 0.0301(13) for the ground-state transition has been obtained from $I_{GS} = 1 - \sum_i I_\beta^i$, $I_{GS}$ and $I_\beta^i$ being the decay branching ratios to the ground state and the level $i$ in $^{37}$K, respectively. This $B(\mathrm{GT})$ agrees very well with that of the $^{37}$Ar(EC)$^{37}$Cl mirror transition (0.0303(8) [1]). Table 2 shows that including the $\beta\gamma$-rates dramatically changes the low-energy $\beta$-decay $B(\mathrm{GT})$ distribution compared to that obtained [6] from $\beta$p data alone.

### 3.1.2 *Lifetimes and decay widths of excited states in $^{37}K$*

Combining the $\beta\gamma$ and $\beta$p intensities measured in this work, we obtain $\Gamma_\gamma/\Gamma_p$=0.54(3) for the state at 2750.4 keV and $\Gamma_\gamma/\Gamma_p$=22(2) for the 3239.3 keV state. The latter value is surprisingly high; $\gamma$-deexcitation of proton-unbound states is expected to compete significantly with proton-emission only for excitation energies near the particle threshold [37] ($S_p(^{37}\mathrm{K})$=1857.77(09) keV [32]). Calculations based on the universal *sd*-shell hamiltonian [1] (USD) can account for this effect at least qualitatively by describing the $J^\pi = \frac{5}{2}^+$ states at 2750.4 and 3239.3 keV as mixtures of the two original USD states [38]. It is possible to explain this mixing by a small adjustment within the uncertainty of the applied residual interaction [39]. With the known resonance strengths $\omega\gamma$ of the $^{36}$Ar(p,$\gamma$)$^{37}$K reaction of 0.208(30) eV [32] and 0.60(15) meV [11] for the states at 2750.4 keV and 3239.3 keV, respectively, and our measured values for $\Gamma_\gamma/\Gamma_p$ we can deduce the partial widths and the corresponding mean lifetimes (see Table 1) using

$$\omega\gamma = \frac{(2J+1)}{(2j_p+1)(2j_t+1)} \frac{\Gamma_p\Gamma_\gamma}{(\Gamma_p+\Gamma_\gamma)}$$

where $J$, $j_p$ and $j_t$ represent the spin of the resonance (i.e. the excited state in $^{37}$K) of the projectile and of the target nucleus, respectively. As can be seen from Table 1, the large $\Gamma_\gamma/\Gamma_p$ value of the 3239 keV state is mainly due to its strongly retarded proton decay. Our mean lifetime for the 2750.4 keV state, $\tau = 2.2(2)$ fs, is consistent with the previous [32] upper limit $\tau < 3$ fs, while our partial $\gamma$-decay widths $\Gamma_\gamma$ differ considerably from the known widths of the mirror states in $^{37}$Ar [32] (these states are particle-bound and have $\Gamma = \Gamma_\gamma$).

### 3.1.3 *Comparison with the $^{37}Cl(p,n)^{37}Ar$ reaction*

Our improved $^{37}$Ca $B$(GT) distribution in Table 2 agrees better with the (p,n) data of Rapaport et al.[7] than does earlier work based solely on $\beta$p spectra. Table 2 also compares our data to preliminary results of a more recent (p,n) measurement [33] that was normalized so that the $^{37}$Cl(p,n)$^{37}$Ar ground-state transition had the $B$(GT) value inferred from the $^{37}$Ar(EC)$^{37}$Cl electron capture rate. We find good agreement of the $B$(GT) values for the transitions into the first excited state, but significant (up to a factor of 5) differences exist for the $^{37}$K states at 2750.4, 3239.3 keV and 3840.2 keV.

These discrepancies are not necessarily surprising. A recent high-sensitivity study of GT strength in $^{38}$Ca $\beta$-decay agreed at the $\pm$20% level with the results extracted from the $^{38}$Ar(p,n)$^{38}$K mirror transitions [40]. However, the transitions showing the good agreement were all quite strong compared to the discrepant ones in A = 37. The weak lowest-lying transition in the A = 38 case had a $\beta$-decay $B$(GT) value which was a factor of 6 larger than that deduced from the (p,n) reaction. It was pointed out [41] that the $B(\mathrm{GT})_{\mathrm{pn}}/B(\mathrm{GT})_{\beta}$ ratio could be different for spin-flip ($d_{3/2} \rightarrow d_{5/2}$) and non-spin-flip (for example $p_{1/2} \rightarrow p_{1/2}$ or $d_{3/2} \rightarrow d_{3/2}$) transitions. This was modeled phenomenologically by adding an effective $\Delta L = 2, \Delta J = 1$ operator, $[Y^{(2)} \otimes \sigma]^{(1)}\tau$. This $\Delta L = 2$ operator can account for the enhancement of the $p_{1/2} \rightarrow p_{1/2}$ and $d_{3/2} \rightarrow d_{3/2}$ transitions [41] as well as the factor of 6 discrepancy found for A = 38 [40]. One might expect that $\Delta L = 2$ contributions to the (p,n) cross-section could affect the inferred $B$(GT) values in A = 37 as well, expecially for the weak low-lying states of Table 2. Therefore, a calibration of the $B(\mathrm{GT})_{\mathrm{pn}}$ function to the ground state transition might not be adequate. Less importantly, one should not necessarily expect the same accuracy in the A = 37 case because in the A = 38 comparison, the $\beta$-decay and (p,n) transitions fed the same final states ($^{38}$K levels in both cases). Hence, we cannot conclusively decide whether the remaining discrepancies between the $^{37}$Ca $\beta$-decay data and the $^{37}$Cl(p,n)$^{37}$Ar results are inherent in the (p,n) reaction mechanism or whether they originate from "real" isospin asymmetries.

### 3.1.4 *Isospin mixing in $^{37}K$*

For the transition into the IAS at 5050.6 keV [6], we obtain $(B(\mathrm{F})+B(\mathrm{GT}))_{IAS} = 2.98(7)$ while the transition into the $J^{\pi}=(\frac{3}{2},\frac{5}{2})^{+}$ level at 5016.1 keV [6], i.e. only 34.5 keV below the IAS, has $(B(\mathrm{F})+B(\mathrm{GT}))_{5016} = 0.123(4)$. It is thus possible that the 5016 keV state is significantly fed by Fermi decay. This conclusion takes into account (i) the model-independent value $B(\mathrm{F})_{\mathrm{total}} = 3$, (ii) that $\gamma$-deexcitation of the IAS has been found to be negligible [6], and (iii) that USD calculations [1] predict $B(\mathrm{GT})_{IAS} = 0.10$. We estimate the uncertainly in the

shell-model prediction from the agreement of the predicted $B$(GT)'s of the analog $T = 1/2$ ground-state to ground-state transitions in A = 35, 37, and 39. As these agree with the data to within $19 \pm 5\%$, $1 \pm 3\%$ and $16 \pm 1\%$, respectively, we assume the "theoretical error bar" on $B(\mathrm{GT})_{IAS}$ is $\pm 0.02$. Accordingly, we conclude that there is evidence, on a level of 1.6 standard deviations, that the decay of $^{37}$Ca to the 5016 keV state in $^{37}$K contains at least some isospin-forbidden Fermi strength. Shell-model calculations [42, 43] of isospin-forbidden Fermi decays, which do a reasonable job of reproducing the seven experimentally known isospin-mixing matrix elements in the *sd* shell, predict a $J^{\pi}=\frac{3}{2}^{+}$ state near the IAS, which is connected to the IAS by an isospin-mixing matrix element of 5.5 keV. If correct, these calculations would imply that the $\beta$-decay strength to 5016 keV level arises predominantly from its admixture with the IAS.

### 3.1.5 *Neutrino capture cross-section of $^{37}$Cl*

We used the $B$(GT)+$B$(F) values from this work to determine the neutrino capture cross-section $\sigma(^{37}\mathrm{Cl})$. In this context, it might be argued that phase-space limitations hinder the accurate extraction of the $B$(GT) function at high excitation energies. However, the $B$(GT) for the strong transition seen at $E_x$ = 7.65 MeV in the (p,n) experiment [7] is quantitatively reproduced by the sum of the $\beta$-decay $B$(GT) values in this region. The neighbouring peak in the (p,n) data at 9.65 MeV is beyond the threshold where $^{37}$Ar becomes effectively unbound against $\alpha$-emission (i.e. $\Gamma \approx \Gamma_{\alpha}$). Since the detection of the neutrino flux by means of the $^{37}$Cl detector is based on counting the produced $^{37}$Ar atoms [5], $^{37}\mathrm{Ar}(\mathrm{e}^{+}\nu,\alpha)^{33}\mathrm{S}$ break-up reactions do not contribute to the measured events. Additionally, due to phase-space arguments the influence of possibly unobserved $B$(GT) strength at high excitation energies on $\sigma(^{37}\mathrm{Cl})$ is very small [44]. In our calculations for $\sigma(^{37}\mathrm{Cl})$, we took the $^{37}$Ar excitation energies in case of known isobaric correspondences [32] and the excitation energies in $^{37}$K for the remaining states. In the latter case, we assumed the mean deviation between the mirror states as the uncertainty of the excitation energies. For the neutrino capture into the ground state of $^{37}$Ar the $B$(GT) value of the $^{37}\mathrm{Ar(EC)}^{37}\mathrm{Cl}$ decay was used.

The dominant part of the predicted solar-neutrino capture rate for the $^{37}$Cl detector is ascribed to those neutrinos originating in the $^{8}$B decay. The corresponding neutrino spectrum was taken from [45]. The $^{37}$Cl capture cross-section for the $^{8}$B neutrinos was calculated by folding this spectrum with the energy-dependent cross-section. Correspondingly, we obtained $\sigma(^{37}\mathrm{Cl})$ for the detection of the neutrinos originating in the $^{3}\mathrm{He}(\mathrm{p},\mathrm{e}^{+}\nu)^{4}\mathrm{He}$ reaction by using the neutrino spectrum given in [44]. For the $^{8}$B cross-section, our result agrees with that obtained previously [6] (see Table 3). This is due to the fact that our experiment reveals *more* transition

strength for the states at low excitation energies but *less* at higher excitation energies. Moreover, the $\sigma(^{37}Cl)$ result obtained in this work agrees very well with the standard value given in [44]. Thus the origin of the discrepancies between the solar neutrino flux predicted by standard model calculations [44] and the value measured with the $^{37}Cl$ detector remains still an open question.

### 3.2 Results for $^{36}Ca$

Figure 8 shows the $\gamma$–spectrum observed for $^{36}Ca$ decay. We were able to identify two strong $\beta\gamma$-transitions into proton-bound states of $^{36}K$ with excitation energies of 1112.8(4) and 1619.0(2) keV while no $\gamma$-deexcitation of proton-unbound levels was observed. As in the case of $^{37}Ca$, the $^{35}Ar$ line originated from the decay of the implanted contaminant $^{35}K$ as well as from the $\beta$p decay of $^{36}Ca$ to the first excited state of $^{35}Ar$ (see below). Six transitions to proton-unbound levels in $^{36}K$ located at 3370(29), 4286(8), 4457(33), 4687(37), 5947(47) and 6798(71) keV were identified in the $\beta$p spectrum (Figure 9). The weak $\beta$p-decays of $^{36}Ca$ into the $^{36}K$ states at 4457 and 4687 keV can be clearly separated from the $\beta$p line originating from the Fermi decay by requiring a small $\beta$-ray energy loss ($\Delta E_\beta \leq 500$ keV) in one of the $\beta$-detectors (see inset in Figure 9). The energies for the 3370(29) keV state and the IAS at 4286(8) keV are weighted means of our values of 3390(41) and 4287(39) keV and the literature data of 3350(40) and 4258(24), 4289(8) keV, respectively [32, 12, 13]. The weak proton line at $E_p \approx 1.37$ MeV was identified as the decay of the IAS in $^{36}K$ to the first excited state of $^{35}Ar$ ($E_x = 1184.2(4)$ keV). This identification is based on the following considerations: (i) the difference of the energies of the two corresponding proton lines is consistent with this assumption; (ii) our rate for this $\gamma$–line is 2.5 $\sigma$ above the experimental value for the $^{35}K$ $\beta$-decay [32] while taking into account the feeding of this state via the decay of the IAS in $^{36}K$ leads to a value consistent with [32]; (iii) the proton spectrum coincident with the $^{35}Ar$ $\gamma$ line shows, in addition to $\beta$-ray energy loss signals, a few events at proton energies of about 1.37 MeV. Accordingly, from the line intensities in the $\beta$p spectrum a value of $\Gamma_{p_1}/\Gamma_{p_0} = 0.03(1)$ was extracted, $p_0$ and $p_1$ being the proton decays of the IAS into the $^{35}Ar$ ground and first excited state, respectively. For the $^{36}Ca$ half-life a value of 102(2) ms was extracted (see Figure 10). The complete $\beta$-decay scheme of $^{36}Ca$ obtained from our work is displayed in Figure 11.

The excitation energies, log$ft$ values and the $B$(GT) function measured in this work are shown in Table 4. The log$ft$ values allow to identify all transitions, except for the Fermi decay, as allowed GT decays, resulting in a $J^\pi = 1^+$ assignment for the corresponding final states in $^{36}K$. For the pure Fermi decay of $^{36}Ca$ into the IAS in $^{36}K$ we obtain $B(F) = 4.05(13)$ which is consistent with the model-independent value $B(F) = (Z - N) = 4$ [1].

Comparing our $J^\pi$ assignment with those of the known levels of the mirror nucleus $^{36}$Cl [32], we can identify the $^{36}$K levels at 1112.8(4) and 1619.0(2) keV as the analog states of the 1164.9 and 1601.1 keV levels in $^{36}$Cl [32], respectively, while clear correspondences cannot be deduced for the $1^+$ states at higher excitation energies in $^{36}$K. Additionally, we conclude that the first excited state in $^{36}$K at 800(15) keV, observed in $^{36}$Ar($^3$He, t)$^{36}$K charge-exchange reactions [46], is the analog of the 788.4 keV level ($J^\pi = 3^+$) in $^{36}$Cl [32]. Because the third excited $1^+$ state in $^{36}$Cl occurs at 2676.4 keV [32] we can exclude a $1^+$ assignment for the $^{36}$K states at 1670(20) and 1890(20) keV [32]. These states lie near the proton threshold and could thus be important resonances in $^{35}$Ar(p, $\gamma$) reactions under stellar conditions. The latter reaction is assumed to be part of the break-out path of the S-Ar-Cl cycle, which leads to the production of heavier elements [47, 48].

### 3.3 Comparison with shell-model theory

First we review the history of the effective hamiltonian in the *sd* shell. By the mid 1960's Kuo and Brown had calculated renormalized G-matrix elements for the *sd* shell [49, 50]. One set of matrix elements was applicable to the A = 18 nuclei with two *sd*-shell particles outside of an $^{16}$O closed shell [50], and another set was applicable to the A = 38 nuclei with two *sd*-shell holes within a $^{40}$Ca closed shell [51]. These G-matrix elements gave qualitative agreement with the experimental A = 18 and A = 38 spectra. When the G-matrix was used to calculate the spectra for the *sd*-shell nuclei with more than two particles or holes, the agreement with the number of observed states was good, but the agreement with the actual energy spectra became worse as the number of particles or holes was increased. The calculated spectra for all these nuclei can be improved by allowing some of the 63 *sd*-shell two-body matrix elements to be parameters in a fit to the experimental energy levels. In general, some linear combinations of these 63 parameters are well determined by the experimental data whereas others are not. By 1977 Chung and Wildenthal [52] had found a "particle" interaction (CWP) for the lower *sd* shell by varying 30 linear combinations of the two-body matrix elements to fit 199 energy levels in the A = 18 – 24 mass region, and a "hole" interaction (CWH) for the upper *sd* shell by varying 20 linear combinations to fit 134 energy levels in the A = 32 – 39 mass region. The least-well-determined linear combinations of matrix elements were fixed at the G-matrix values – the "Sum" value from Table 7 of Ref. [50] and the "12.5p" value from Table I of Ref. [51] for the particle and hole systems, respectively. The CWP and CWH interactions work well at their respective ends of the *sd* shell, but when they are extrapolated into the middle (A = 25 – 31) they do not quite match and the agreement with experiment worsens [52]. It

was soon found that a "universal" hamiltonian (the USD interaction [2]) could be obtained by fitting all of the data simultaneously and by introducing a smooth mass dependence of $A^{-0.3}$ into the matrix elements. The USD interaction was obtained by varying 47 best-determined linear combinations of parameters to fit 447 energy levels in the mass region A = 18 – 39. The 19 least-well-determined linear combinations were fixed to the A = 18 Kuo G-matrix [50]. The mass dependence is an approximate way of taking into account the interpolation between the A = 18 and A = 38 G-matrix. The differences between the fitted two-body matrix elements and the original G-matrix are attributed to many-body effects not included in the G-matrix calculation, such as effective three-body interactions and low-lying core excitations from $^{16}$O and $^{40}$Ca [2]. Even though the difference between the empirical matrix elements and G-matrix is not large, the effect of the difference builds up quickly with particle (or hole) number, and it is crucial to take into account the empirical adjustments to obtain agreement with spectroscopic data [2, 52].

The GT $\beta$ decay and electromagnetic properties throughout the *sd* shell are well described by the USD interaction [1, 2], as long as effective operators are used for the GT $\beta$-decay and electromagnetic operators. These effective operators arise from the non-*sd* shell components of the actual wave functions, and the empirical values which are needed to reproduce the experimental data are in qualitative agreement with microscopic calculations which take into account the core-polarization and mesonic exchange contributions [2]. In particular, it is observed that the experimental $\beta$-decay strengths are uniformly reduced from the calculated value. The effective $\sigma\tau$ operator which accounts for this "quenching" and which has the expected mass dependence has the form [1, 2] (ignoring the small orbital and tensor contributions)

$$(\sigma\tau)_{\rm eff} = \left(1 - 0.23\left(\frac{\rm A}{28}\right)^{0.35}\right)(\sigma\tau)_{\rm free}.$$

This approximate effective operator gives a 40% reduction in the middle of the *sd* shell and a 45% reduction in the upper *sd* shell. The full effective GT operator from [1, 2] leads to a 50% reduction in the GT $\beta$-decay strength in the upper *sd* shell. The GT strength calculated with both interactions and the full effective GT operator is compared to the experimental data for $^{38}$Ca [40], $^{37}$Ca (this experiment) and $^{36}$Ca (this experiment) in Figures 12 – 14. For the first state in $^{38}$Ca and the low-lying states up to 5 MeV in excitation energy (in the K daughter nuclei), the agreement between USD and experiment is excellent. At higher excitation energy the USD calculations are significantly smaller than the experiment – a comparison which led one of the earlier works on the $^{37}$Ca decay to question whether the GT strength was actually quenched [8]. One can also compare the experimental results to those obtained with the CWH interaction – the agreement with the lowest states is somewhat worse, but the overall agreement

is somewhat better, as pointed out in [53], due to a downward shift in the position of the main peak in the GT strength function. (Similar conclusions have also been made from a comparison of $^{33}$Ar $\beta$-delayed proton data to predictions based on the USD and CWH hamiltonians [54]).

From the above discussion about the origin of the *sd*-shell hamiltonians, it is clear that both the CWH and USD interactions should be considered for the upper *sd* shell, and that the difference between the two indicates the "theoretical error" in due to the effective interactions. Indeed, the theory is consistent with the data within this theoretical error. To determine the origin of the quenching of GT strength it is crucial to have the experimental data for $^{37}$Ca and $^{36}$Ca "beyond the Q-value window" (where the data in Figure 13 stop). This may be inferred from (p,n) reactions on the mirror N = 20 nuclei $^{37}$Cl and $^{36}$S, respectively. Such experimental data for $^{38}$Ca (the points in Figure 12 above 5 MeV) inferred from the $^{38}$Ar(p, n) reaction data [40] give a total GT strength that is consistent with the quenching expected from the effective GT operator. A quantitative extraction of the GT matrix elements from the (p,n) data must take into account the difference between the effective $\beta$-decay and (p,n) operators discussed in Section 3.1.3.

The existing effective interactions were determined from low-lying energy levels; the part of the interaction that connects the $d_{3/2}$ and $d_{5/2}$ orbitals and which is responsible for the position of the GT resonance was not strongly constrained by experimental data (e.g. one of the least-well-determined linear combinations of parameters) and therefore relied largely on the G-matrix. The CWH interaction may be more appropriate for the upper *sd* shell, because its least-well-determined linear combinations of two-body matrix elements were replaced by the Kuo G-matrix elements calculated explicitly for the upper part (A = 38) of the *sd* shell. The USD interaction provides a better overall adjustment of the interaction for the entire *sd* shell as well as the low-lying states in the upper *sd* shell, but relies only on the Kuo-Brown A = 18 G-matrix for the undetermined linear combinations. The following suggestions for further improvement are clear from this discussion: (i) data on the position of the GT resonance should be included in determining the interaction and (ii) one should replace the least-well-determined linear combinations of two-body matrix elements by G-matrix elements that are interpolated between A = 18 and A = 38 (rather than fixed at the A = 18 values as they are for USD interaction).

# 4 Summary and outlook

Our $^{37}$Ca data have drastically reduced previous discrepancies between the $\beta$-decay and $^{37}$Cl(p,n)$^{37}$Ar results; the inclusion of previously neglected strong $\beta\gamma$-contributions in the $^{37}$Ca decay significantly changes the low-energy $B$(GT) distribution. However, factor of two differences between

$\beta$-decay and (p,n) GT strengths remain. There appears to be a significant isospin-forbidden Fermi component in the decay of $^{37}$Ca to the 5016 keV state of $^{37}$K. It should be possible to clarify this effect in a high-resolution study of $^{37}$Ca $\beta$p decay. Such an experiment would make use of $\beta$–$\nu$ angular correlations which produce significantly different line shapes for Fermi and GT transitions in $\beta$p spectra [55]. The $\sigma(^{37}\mathrm{Cl})$ values found in this work agree with the values used in standard solar model calculations [44] and thus give no hints for a solution of the solar neutrino problem. In conclusion, we have shown that combining high-precision decay studies of the same nucleus at an ISOL mass separator and at a fragment separator facilitates possible precise and detailed study of nuclear decay far from the stability valley.

Our $^{36}$Ca work gave a complete $B$(GT) distribution for the heaviest $\mathrm{T_z} = -2$ nucleus where such information is available. The term "complete" refers to the fact that both $\beta$-delayed protons and $\gamma$-rays were observed, that the normalization of the branching ratios was achieved by counting parent atoms as well as their decays, that high precision was obtained for the half-life, and that a reasonably sensitive upper limit was placed on unobserved $B$(GT) strength up to 6.8 MeV. It would be very interesting to perform a high-resolution measurement of the $\beta$p spectrum of the $^{36}$Ca decay with particular emphasis on the GT strength at high excitation energies. Last but not least, a study of the $^{36}$S(p,n)$^{36}$Cl reaction would help to clarify the discrepancies between $\beta$-decay and the (p,n) reaction data.

We have compared the experimental results to *sd*-shell calculations using an effective GT operator [1] and the CWH and USD hamiltonians. These give Gamow-Teller strength distributions that differ considerably at higher excitation energy due to an energy shift in the GT strength distribution. The experimental results generally lie in between the two calculations. To further improve the *sd*-shell hamiltonian, one will have to include data on the energy of these GT distributions and incorporate more realistic models of the least-well-determined combinations of parameters.

## Acknowledgements

EGA thanks CERN for support as a Paid Scientific Associate, ZJ acknowledges support from the Alexander von Humboldt Foundation, and BAB acknowledges support from NSF grant 94-03666. The authors from Warsaw are grateful for the support and hospitality of GSI and partial support from Polish Committee of Scientific Research KBN under grant 2P30214806.

## References


[1] B.A. Brown and B.H. Wildenthal, At. Data Nucl. Data Tables 33 (1985) 347.

[2] B.A. Brown and B.H. Wildenthal, Ann. Rev. Nucl. Part. Sci. 38 (1988) 29.

[3] E. Roeckl, Rep. Prog. Phys. 55 (1992) 1661.

[4] G. Audi and A.H. Wapstra, Nucl. Phys. A 565 (1993) 1.

[5] R. Davis, D.S. Harmer and K.C. Hoffman, Phys. Rev. Lett. 20 (1968) 1205.

[6] A. Garcia, E.G. Adelberger, P.V. Magnus, H.E. Swanson, O. Tengblad and the ISOLDE Collaboration and D.M. Moltz, Phys. Rev. Lett. 67 (1991) 3654, A. Garcia, Ph.D. thesis, University of Washington (1991).

[7] J. Rapaport, T.N. Taddeucci, P. Welch, C. Gaarde, J. Larsen, C.D. Goodman, C.C. Foster, C.A. Goulding, D. Horen, E.R. Sugarbaker and T. Masterson, Phys. Rev. Lett. 47 (1981) 1518.

[8] E.G. Adelberger, A. Garcia, P.V. Magnus and D.P. Wells, Phys. Rev. Lett. 67 (1991) 3658.

[9] D. Wells, E.G. Adelberger, P.V. Magnus, C.D. Goodman, Y. Wang, B. Ni, A. Smith, J. Rapaport, B.K. Park, X. Wang, L. Wang, E.R. Sugarbaker, D. Marchelenski, B. Luther, S. de Lucia, T.N. Taddeucci, L.J. Rybarcyk, R. Byrd and D. Aschman, Bull. Am. Phys. Soc. 37 (1992) 1296.

[10] P.V. Magnus, E.G. Adelberger and N. Cabot, Phys. Rev. C 51 (1995) 2806.

[11] C. Iliadis, J. Höhne, F. Käppeler, J. Meissner, H.P. Trautwetter and M. Wiescher, Phys. Rev. C 48 (1993) R1479.

[12] J. Äystö, M.D. Cable, R.F. Parry, J.M. Wouters, D.M. Moltz and J. Cerny, Phys. Rev. C 23 (1981) 879.

[13] A. Garcia, E.G. Adelberger, P.V. Magnus, H.E. Swanson, F.E. Wietfeldt, O. Tengblad and the ISOLDE Collaboration, Phys. Rev. C 51 (1995) 3487.

[14] W. Trinder, E.G. Adelberger, Z. Janas, H. Keller, K. Krumbholz, V. Kunze, P. Magnus, F. Meissner, M. Pfützner, E. Roeckl, K. Rykaczewski, W.-D. Schmidt-Ott and M. Weber, GSI Sci. Rep. 1993, GSI-94-1 (1994) 51.

[15] W. Trinder, E.G. Adelberger, Z. Janas, H. Keller, K. Krumbholz, V. Kunze, P. Magnus, F. Meissner, M. Pfützner, E. Roeckl, K. Rykaczewski, W.-D. Schmidt-Ott and M. Weber, Proc. Int. Conf. on nuclear shapes and nuclear structure at low excitation energies, Antibes, 1994, eds. M. Verges, D. Goutte, P.H. Heenen and J. Sauvage (Editions Frontières, 1994) p. 479.

[16] W. Trinder, E.G. Adelberger, Z. Janas, H. Keller, K. Krumbholz, V. Kunze, P. Magnus, F. Meissner, M. Pfützner, E. Roeckl, K. Rykaczewski, W.-D. Schmidt-Ott and M. Weber, Proc. Tours symposium on nuclear physics II, Tours, 1994, eds. H. Utsunomiya, M. Ohta, J. Galin and G. Münzenberg (World Scientific, 1995) p. 550.

[17] W. Trinder, E.G. Adelberger, B.A. Brown, Z. Janas, H. Keller, K. Krumbholz, V. Kunze, P. Magnus, F. Meissner, M. Pfützner, E. Roeckl, K. Rykaczewski, W.-D. Schmidt-Ott and M. Weber, GSI Sci. Rep. 1994, GSI-95-1 (1995) 24.

[18] W. Trinder, E.G. Adelberger, B.A. Brown, Z. Janas, H. Keller, K. Krumbholz, V. Kunze, P. Magnus, F. Meissner, M. Pfützner, E. Roeckl, K. Rykaczewski, W.-D. Schmidt-Ott and M. Weber, Phys. Lett. B 348 (1995) 331.

[19] W. Trinder, E.G. Adelberger, Z. Janas, H. Keller, K. Krumbholz, V. Kunze, P. Magnus, F. Meissner, M. Pfützner, E. Roeckl, K. Rykaczewski, W.-D. Schmidt-Ott and M. Weber, Phys. Lett. B 349 (1995) 267.

[20] W. Trinder, E.G. Adelberger, B.A. Brown, Z. Janas, H. Keller, K. Krumbholz, V. Kunze, P. Magnus, F. Meissner, M. Pfützner, E. Roeckl, K. Rykaczewski, W.-D. Schmidt-Ott and M. Weber, Proc. Int. Conf. on Exotic Nuclei and Atomic Masses, Arles, 1995, eds. M. de Saint Simon and O. Sorlin (Editions Frontières, 1995) p. 751.

[21] H. Geissel, P. Armbruster, K.-H. Behr, A. Brünle, K. Burkhard, M. Chen, H. Folger, B. Franczak, H. Keller, O. Klepper, B. Langenbeck, F. Nickel, E. Pfeng, M. Pfützner, E. Roeckl, K. Rykaczewski, I. Schall, D. Schardt, C. Scheidenberger, K.-H. Schmidt, A. Schröter, T. Schwab, K. Sümmerer, M. Weber, G. Münzenberg, T. Brohm, H.-G. Clerc, M. Fauerbach, J.-J. Gaimard, A. Grewe, E. Hanelt, B. Knödler, M. Steiner, B. Voss, J. Weckenmann, C. Ziegler, A. Magel, H. Wollnik, J.P. Dufour, Y. Fujita, D.J. Vieira and B. Sherill, Nucl. Instr. and Meth. B 70 (1992) 286.

[22] E. Hanelt, Ph.D. thesis, Technische Hochschule Darmstadt (1991).

[23] M. Weber, Ph.D. thesis, Technische Hochschule Darmstadt (1993).

[24] M. Pfützner, B. Voss, H.-G. Clerc, H. Geissel, G. Münzenberg, F. Nickel, K.-H. Schmidt, M. Steiner, K. Sümmerer and D.J. Vieira, GSI Annual Report 1990, GSI-91-1 (1991) 288.

[25] M. Steiner, Diploma work, Technische Hochschule Darmstadt (1991).

[26] W. Trinder, Ph.D. thesis, Universität Frankfurt a.M. (1995).

[27] W. Shen, B. Wang, J. Feng, W. Zhan, Y. Zhu and E. Feng, Nucl. Phys. A 491 (1989) 130.

[28] N.B. Gove and M.J. Martin, Nucl. Data Tables 10 (1971) 205.

[29] A. Piechaczek, Ph.D. thesis, Technische Hochschule Darmstadt (1994).

[30] B.D. Wilkins, M.J. Fluss, S.B. Kaufman, C.E. Gross and E.P. Steinberg, Nucl. Instr. and Meth. 92 (1971) 381.

[31] H. Junde, Nuclear Data Sheets 67 (1992) 523.

[32] P.M. Endt, Nucl. Phys. A521 (1990) 1.

[33] A. Garcia, E.G. Adelberger, P.V. Magnus, H.E. Swanson, F.E. Wietfeldt, O. Tengblad and the ISOLDE Collaboration, Phys. Rev. C 51 (1995) R439.

[34] W.R. Leo, Techniques for Nuclear and Particle Physics Experiments (Springer Verlag, Berlin, 1992) p. 34.

[35] D.H. Wilkinson, Nucl. Instr. Meth. A335 (1993) 172, 201.

[36] D.H. Wilkinson and B.E.F. Macefield, Nucl. Phys. A232 (1974) 58.

[37] C.E. Rolfs and W.S. Rodney, Cauldrons in the Cosmos (The University of Chicago Press, Chicago, 1988) p. 169.

[38] M.B. Aufderheide, S.D. Bloom, D.A. Resler and C.D. Goodman, Phys. Rev. C 49 (1994) 678.

[39] B.A. Brown, unpublished.

[40] B.D. Anderson, A.R. Baldwin, P. Baumann, B.A. Brown, F. Didierjean, C.C. Foster, L.A.C. Garcia, A. Huck, A. Knipper, R. Madey, D.M. Manley, G. Marguier, M. Ramdhane, H. Ravn, C. Richard-Serre, G. Walter and J.W. Watson, Phys. Rev. C54, (1996) 602.

[41] J.W. Watson, W. Pairsuwan, B.D. Anderson, A.R. Baldwin, B.S. Flanders, R. Madey, R.J. McCarthy, B.A. Brown, B.H. Wildenthal and C.C. Foster, Phys. Rev. Lett. 55 (1985) 1369.

[42] S. Nakamura, K. Muto and T. Oda, Nucl. Phys. A 575 (1994) 1.

[43] E. Ormand, private communication.

[44] J.N. Bahcall, Neutrino Astrophysics (Cambridge University Press, Cambridge, 1989) p. 198.

[45] J.N. Bahcall and B.R. Holstein, Phys. Rev. C 33 (1986) 2121.

[46] T.G. Dzubay, A.A. Jaffe, E.J. Ludwig, T.A. White, F. Everling, D.W. Miller and D.A. Outlaw, Phys. Lett. B 33 (1970) 302.

[47] L. van Wormer, J. Görres, C. Iliadis, M. Wiescher and F.K. Thielemann, Ap. J. 432 (1994) 326.

[48] F. Rembges, C. Freiburghaus, T. Rauscher, F.K. Thielemann, H. Schatz and M. Wiescher, Ap. J.,in print.

[49] T.T.S. Kuo and G.E. Brown, Nucl. Phys. 85 (1966) 40.

[50] T.T.S. Kuo, Nucl. Phys. A103 (1967) 71.

[51] B.H. Wildenthal, E.C. Halbert, J.B. McGrory and T.T.S. Kuo, Phys. Rev. C4, (1971) 1266.

[52] W. Chung, Ph.D. thesis, Michigan State Univ., 1976; B.H. Wildenthal in "Elementary Modes of Excitation in Nuclei", Proceedings of the International School of Physics "Enrico Fermi", course 69, edited by A. Bohr and R.A. Broglia (North-Holland, 1977), p. 383; B.H. Wildenthal and W. Chung in "Mesons in Nuclei", edited by M. Rho and D.H. Wilkinson, (North-Holland, 1979), p. 723.

[53] B.A. Brown, Phys. Rev. Lett. 69 (1992) 1034.

[54] A. Honkanen et al., Nucl. Phys. A611, 47 (1996).

[55] D. Schardt and K. Riisager, Z. Phys. A345 (1993) 265.

Figure 1: Experimental setup, (a) overview of the projectile fragment separator FRS at GSI, (b) instrumentation at the final focus of the FRS, (c) detectors for decay spectroscopy.

Figure 2: Measured range distribution of the $^{37}$Ca atoms in the implantation detector. The width (FWHM) of the Gaussian curve is approximately 100 $\mu$m. The figure does not show the full statistics obtained in the experiment.

Figure 3: Energy-loss distribution of transmitted atoms, measured by the MUSIC detector for the FRS setting on $^{37}$Ca. The figure does not show the full statistics obtained in the experiment.

Figure 4: $^{37}$Ca decay time distribution obtained from its $\beta$-delayed proton emission. The curve fitted to the data yields a half-life of $181.1 \pm 1.0$ ms.

Figure 5: $\gamma$-spectrum from $^{37}$Ca decay measured in coincidence with $\beta$-rays recorded in the implantation detector. The dominant lines are labeled by the nuclides in which the transitions occur. The $^{36}$Ar $\gamma$-rays originate mainly from the $\beta$-decay of the implanted contaminant $^{36}$K, but also from the $\beta$p decay of $^{37}$Ca into excited states of $^{36}$Ar. The lower intensity lines are due to weaker transitions in $^{36}$Ar or to single or double escape effects.

Figure 6: Proton spectrum from $^{37}$Ca decay, measured by the implantation detector; (a) raw spectrum, (b) spectrum in coincidence with a $\beta$-ray detected in the downstream $\beta$-detector, (c) same as (b) but with an additional condition on a small $\beta$-ray energy deposit ($\Delta E_\beta \leq 450$ keV) in the downstream $\beta$-detector (see text).

Figure 7: $^{37}$Ca $\beta$-decay scheme.

Figure 8: $\gamma$-spectrum from $^{36}$Ca decay, measured in coincidence with $\beta$-rays in the implantation detector. The dominant lines are labeled by the nuclides in which the transitions occur. The $^{35}$Ar $\gamma$-rays originate from the $\beta$-decay of the implanted contaminant $^{35}$K as well as from the $\beta$p decay of $^{36}$Ca into the first excited state of $^{35}$Ar.

Figure 9: Proton spectrum from $^{36}$Ca decay, measured by the implantation detector. The inset shows part of the spectrum obtained under the condition of a small $\beta$-ray energy deposit ($\Delta E_\beta \leq 500$ keV) in the downstream $\beta$-detector (see text).

Figure 10: $^{36}$Ca decay time distribution obtained from its $\beta$-delayed proton emission. The curve fitted to the data yields a half-life of $102 \pm 2$ ms.

Figure 11: $^{36}$Ca $\beta$-decay scheme.

Figure 12: Comparison of the measured $B$(GT) strength in $^{38}$Ca $\beta$-decay [40] with shell-model predictions. The integrated $B$(GT) strength is shown as a function of the excitation energy in $^{38}$K for the experimental values (points) and for *sd*-shell model calculations using the USD interaction (straight line) and the CWH interaction (dashed line).

Figure 13: Comparison of the measured $B$(GT) strength in $^{37}$Ca $\beta$-decay with shell-model predictions. The integrated $B$(GT) strength is shown as a function of the excitation energy in $^{37}$K for the experimental values (points) and for *sd*-shell model calculations using the USD interaction (straight line) and the CWH interaction (dashed line).

Figure 14: Comparison of the measured $B$(GT) strength $^{36}$Ca $\beta$-decay with shell-model predictions. The integrated $B$(GT) strength is shown as a function of the excitation energy in $^{36}$K for the experimental values (points) and for *sd*-shell model calculations using the USD interaction (straight line) and the CWH interaction (dashed line).

Table 1: Decay widths and lifetimes of excited states in $^{37}$K and $^{37}$Ar.

| $E_x(^{37}K)$/keV | $\Gamma_p(^{37}K)$/eV | $\Gamma_\gamma(^{37}K)$/eV | $\tau(^{37}K)$/fs | $\Gamma(^{37}Ar)$/eV [32] |
|---|---|---|---|---|
| 2750.4 | 0.20(3) | 0.11(2) | 2.2(2) | 0.033(10) |
| 3239.3 | $2.1(6)\times10^{-4}$ | $4.6(1.2)\times10^{-3}$ | 140(40) | $8(1)\times10^{-3}$ |

Table 2: $B$(GT) strength at low excitation energies in $^{37}$K. The values taken from [6, 33, 9] were divided by $(g_A/g_V)^2 = (1.262)^2$ because of a different definition of $B$(GT) in these references.

| $E_x(^{37}K)$/MeV | $\beta$-decay (this work) | $\beta$-decay [6] | $\beta$-decay [33] | (p,n) [7] | (p,n)[a] [9, 33] |
|---|---|---|---|---|---|
| 0.0 | 0.0301(13)[b] | | | 0.034(7) | |
| 1.3709 | 0.0079(4) | 0.046(6)[b] | 0.0058(16) | < 0.009 | 0.0088(6) |
| 2.7504 | 0.064(2) | 0.042(3) | 0.075(6) | | 0.0440(13) |
| 3.2393 | 0.055(3) | 0.0024(6) | 0.051(10) | | 0.080(3) |
| 3.6222 | 0.0458(13) | 0.047(3) | 0.047(3) | | 0.036(2) |
| 3.8402 | 0.058(2) | 0.059(3) | 0.059(3) | | 0.0119(6) |
| 2–4 | 0.223(4) | 0.151(5) | 0.233(13) | 0.23(4) | |

[a] preliminary values (see text)

[b] deduced from intensity balance (see text)

Table 3: Solar neutrino cross-sections $\sigma$ for the $^{37}$Cl detector. Depicted are only the values for those neutrino sources whose detection is affected by transitions into excited states of $^{37}$Ar. All values are given in units of $10^{-42}$cm$^2$.

| neutrino source | $\sigma_{\beta-\text{decay}}$ (this work) | $\sigma_{\beta-\text{decay}}$ [6] | $\sigma_{\text{standard}}$ [44, 45] |
|---|---|---|---|
| $^8\text{B} \rightarrow {}^8\text{Be}^* + \text{e}^+ + \nu$ | 1.09(3) | 1.09(3) | 1.06(10) |
| $^3\text{He} + \text{p} \rightarrow {}^4\text{He} + \text{e}^+ + \nu$ | 4.23(10) | 4.26(15) | 3.9 |

Table 4: Excitation energy, log$ft$ and $B$(GT) values for the $^{36}$Ca $\beta$-decay, measured in this work.

| $E_x(^{36}\text{K})$/keV | log$ft$ | $B$(GT) |
|---|---|---|
| 1112.8(4) | 4.56(6) | 0.11(2) |
| 1619.0(2) | 4.08(5) | 0.32(4) |
| 3370(29) | 4.02(3) | 0.36(2) |
| 4286(8) | 3.18(2) | |
| 4457(33) | 4.49(5) | 0.13(2) |
| 4687(37) | 4.47(5) | 0.13(2) |
| 5947(47) | 3.65(8) | 0.9(2) |
| 6798(71) | 3.8(1) | 0.6(2) |

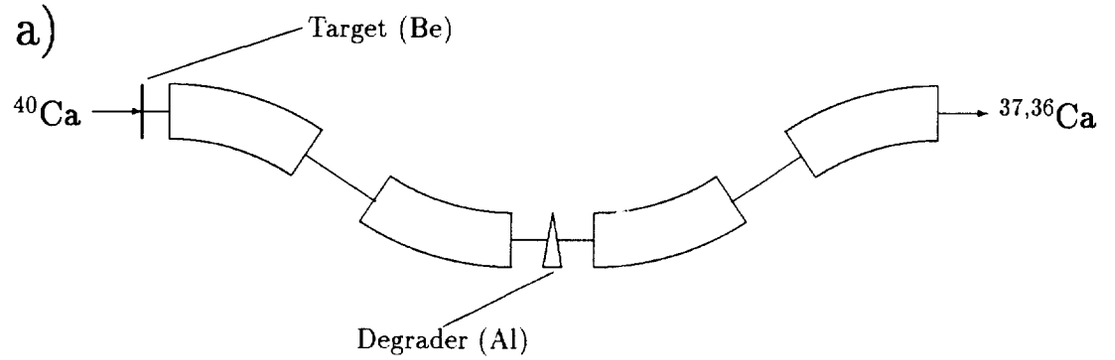
a)
Target (Be)
$^{40}$Ca
$^{37,36}$Ca
Degrader (Al)

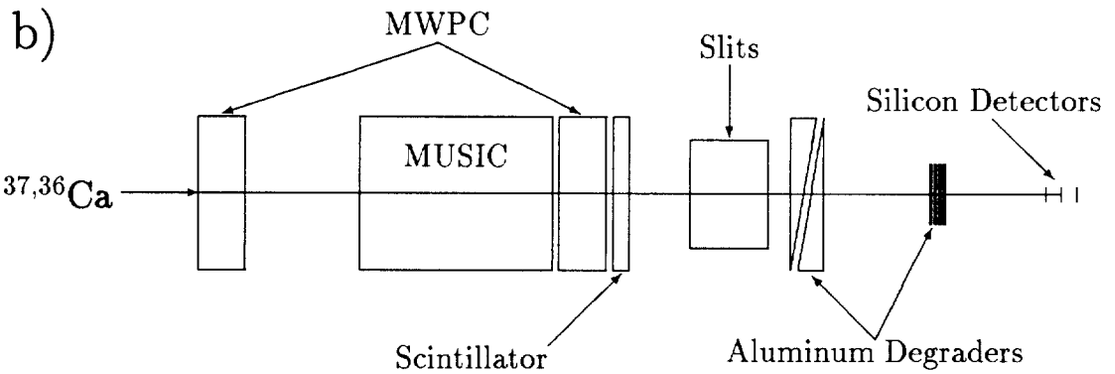
b)
MWPC
Slits
Silicon Detectors
MUSIC
$^{37,36}$Ca
Scintillator
Aluminum Degraders

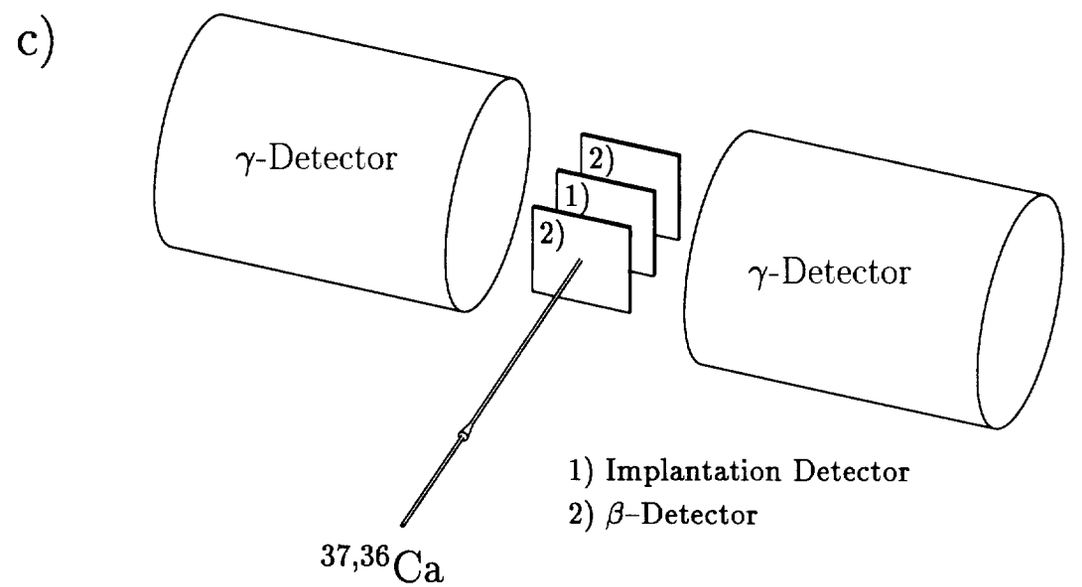
c)
γ-Detector
2)
1)
2)
γ-Detector
1) Implantation Detector
2) β–Detector
$^{37,36}$Ca

Fig. 1

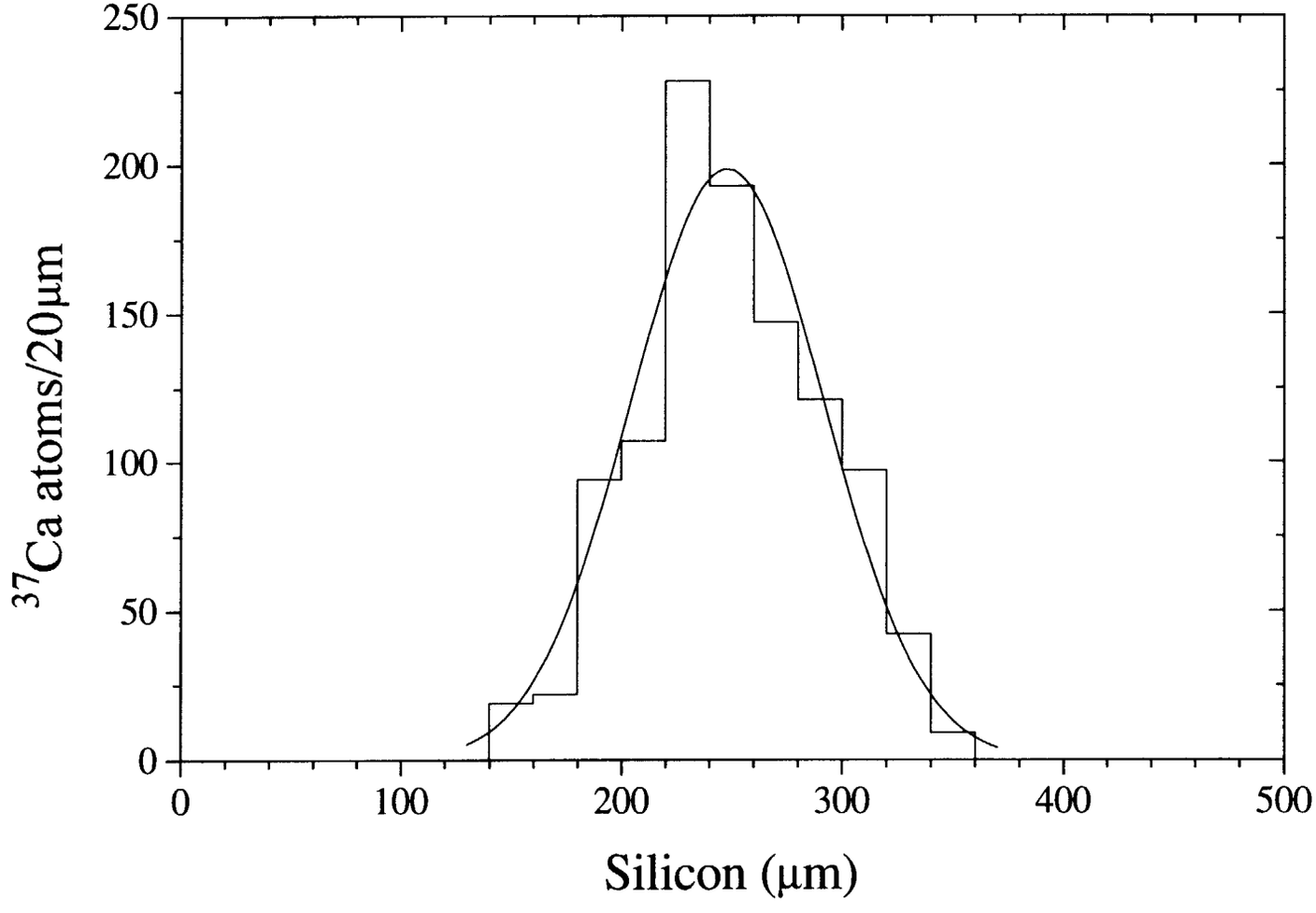
250
200
150
100
50
0
$^{37}$Ca atoms/20μm
0
100
200
300
400
500
Silicon (μm)

Fig 2

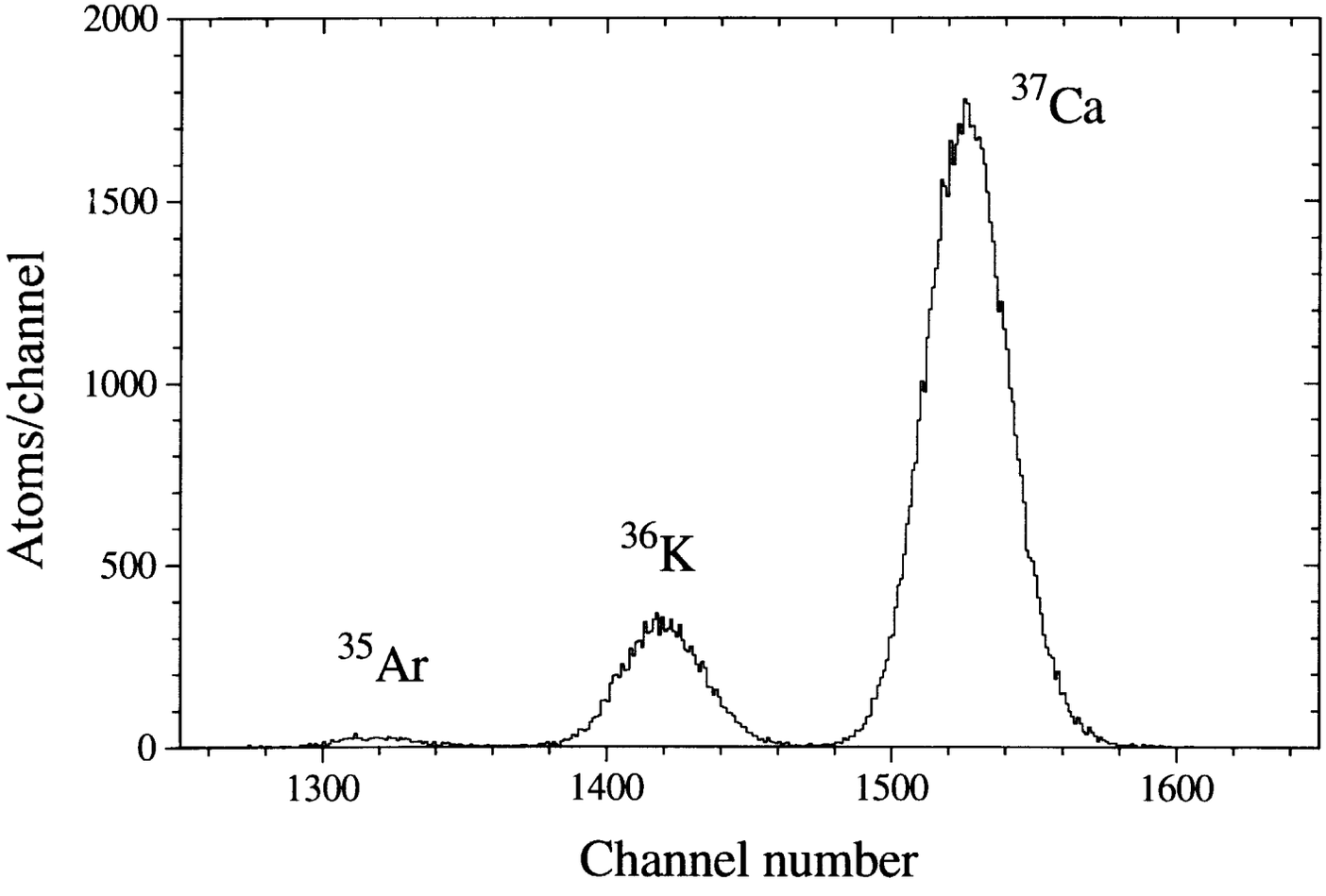
2000
1500
1000
500
0
Atoms/channel
$^{37}$Ca
$^{36}$K
$^{35}$Ar
1300
1400
1500
1600
Channel number

Fig. 3

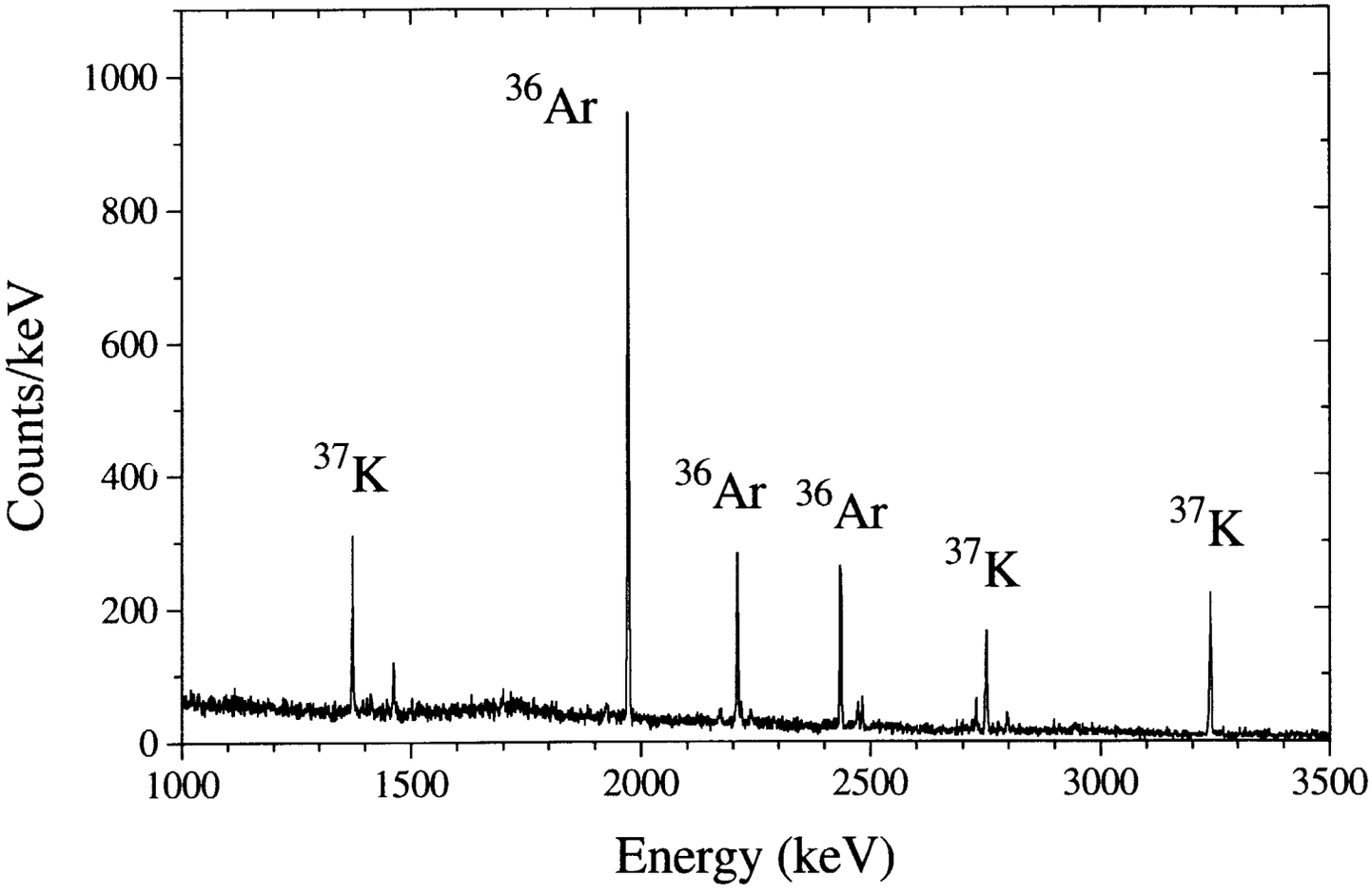
Counts/keV
1000
800
600
400
200
0
1000
1500
2000
2500
3000
3500
Energy (keV)
$^{37}$K
$^{36}$Ar
$^{36}$Ar
$^{36}$Ar
$^{37}$K
$^{37}$K

Fig. 4

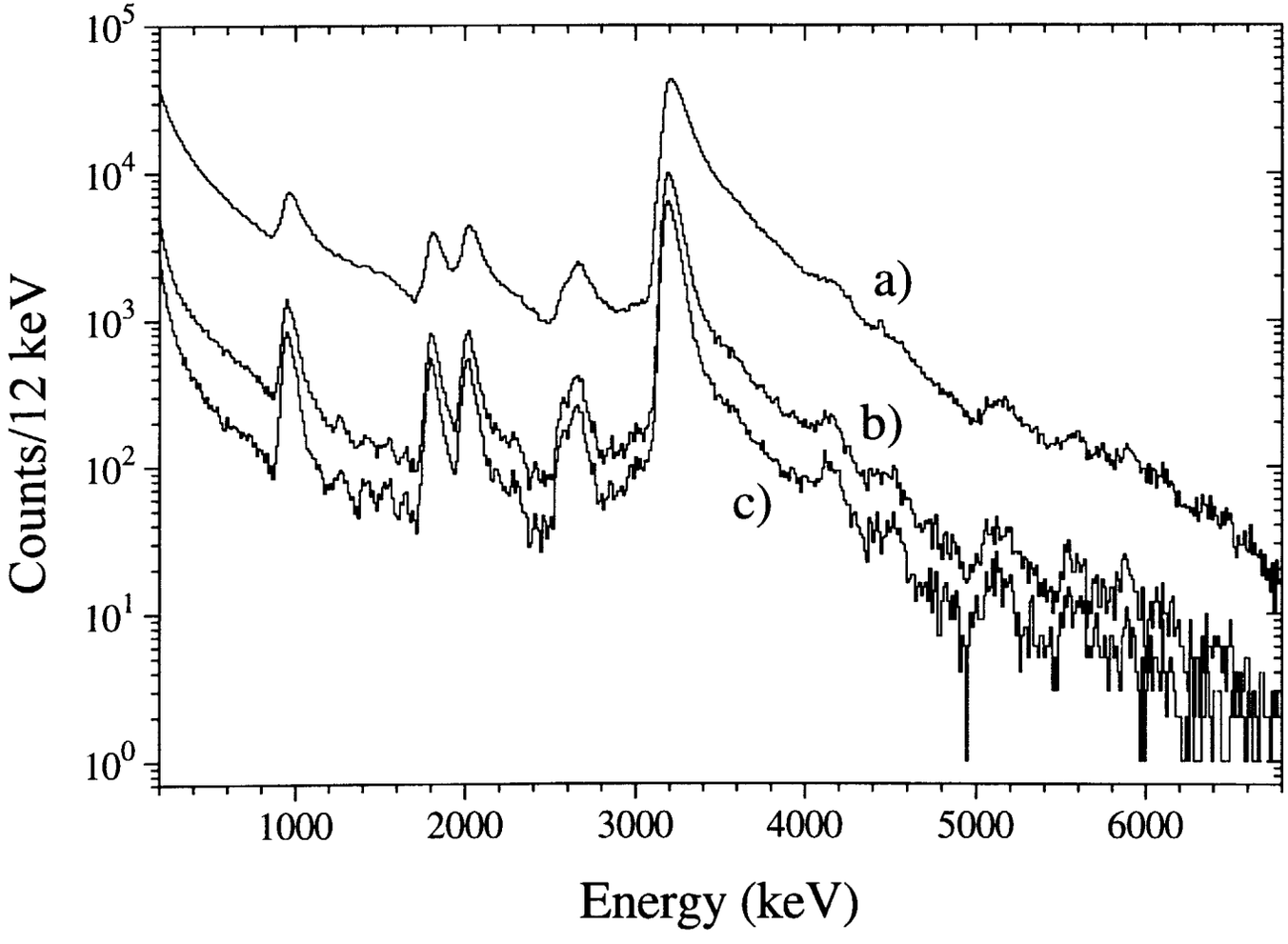
Counts/12 keV
Energy (keV)
a)
b)
c)
$10^0$
$10^1$
$10^2$
$10^3$
$10^4$
$10^5$
1000
2000
3000
4000
5000
6000

Fig. 5

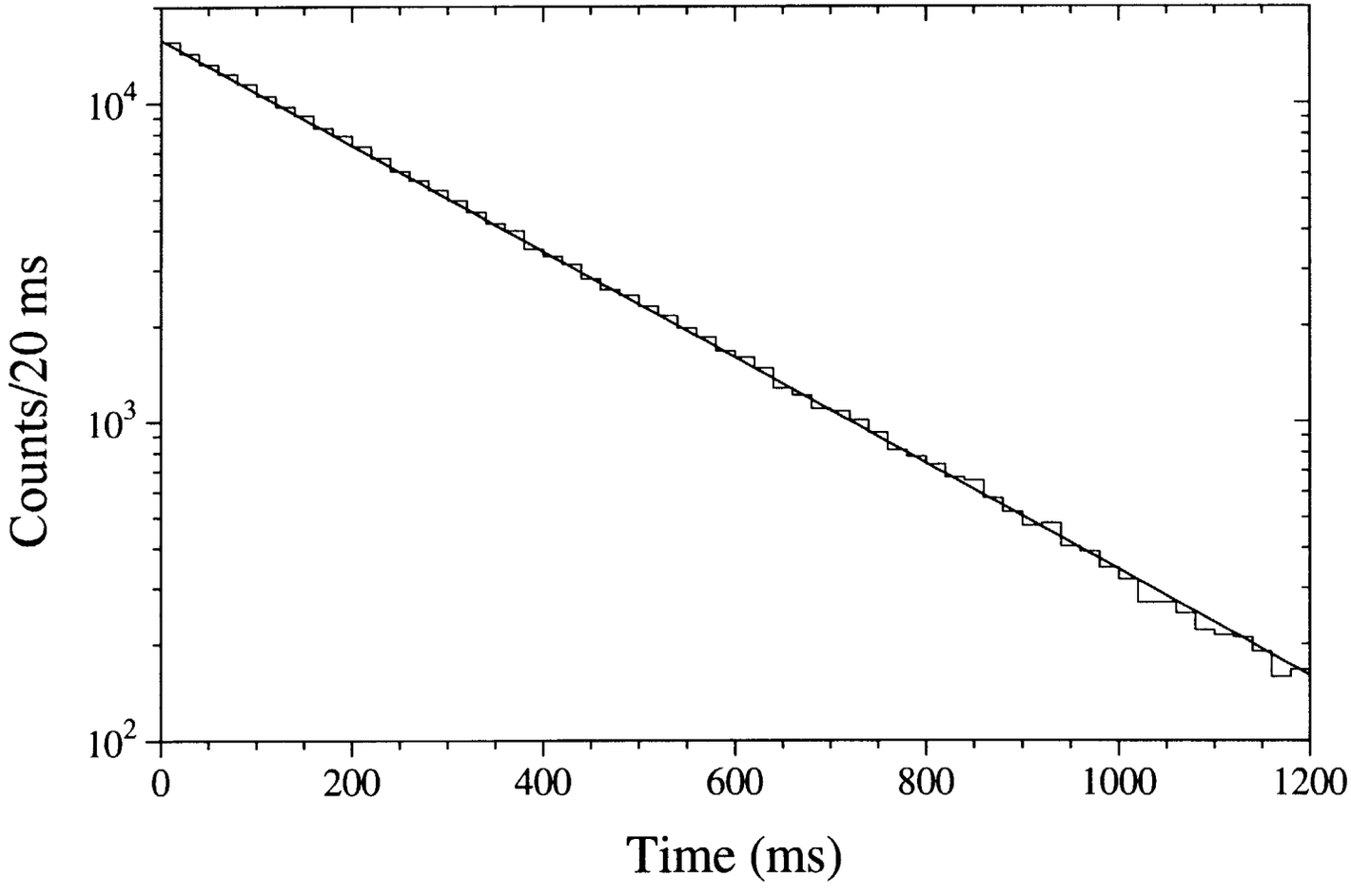


Fig. 6

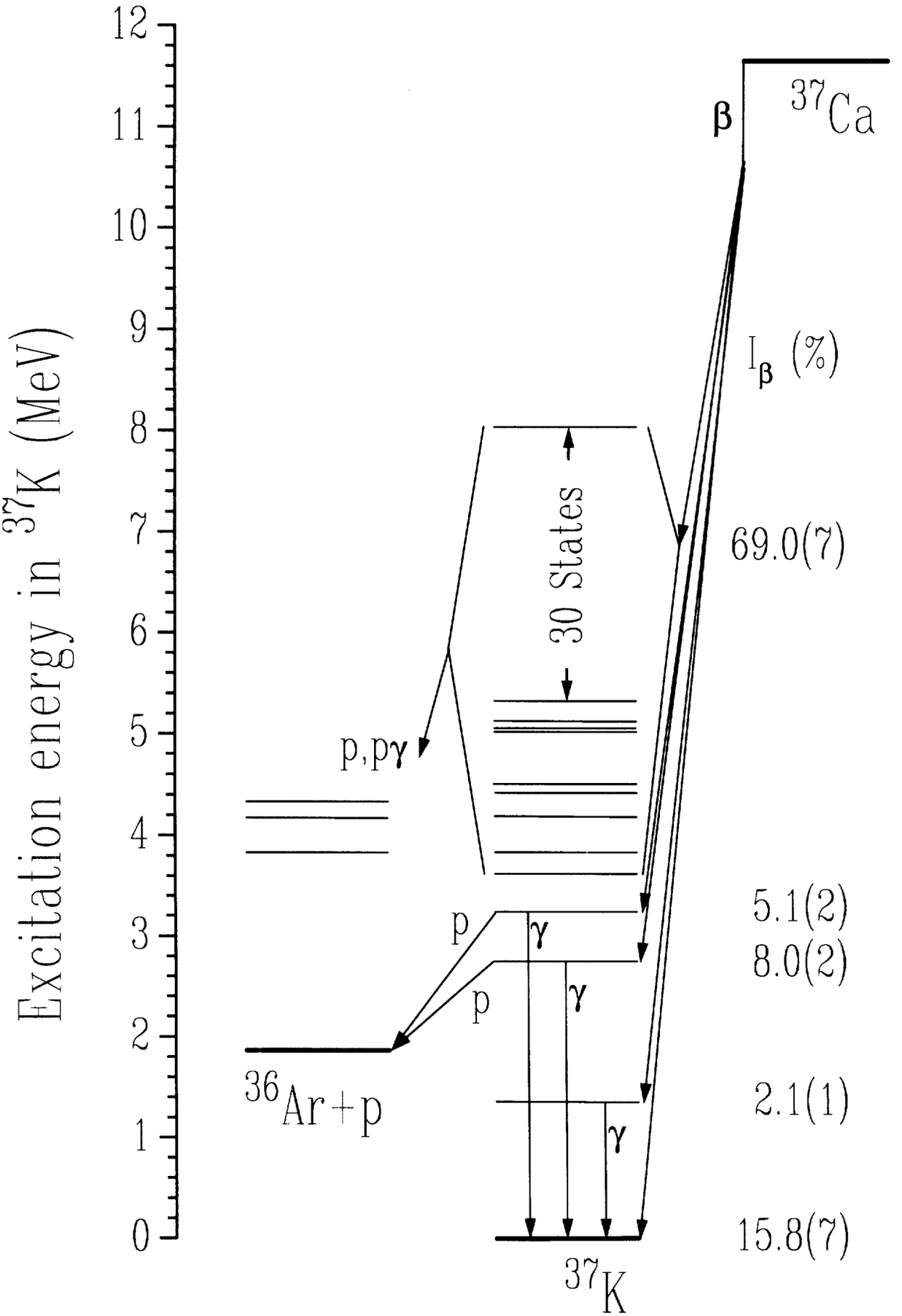
Excitation energy in $^{37}$K (MeV)
12
11
10
9
8
7
6
5
4
3
2
1
0
β
$^{37}$Ca
$I_β$ (%)
69.0(7)
30 States
p,pγ
5.1(2)
8.0(2)
p
γ
p
γ
$^{36}$Ar+p
2.1(1)
γ
15.8(7)
$^{37}$K

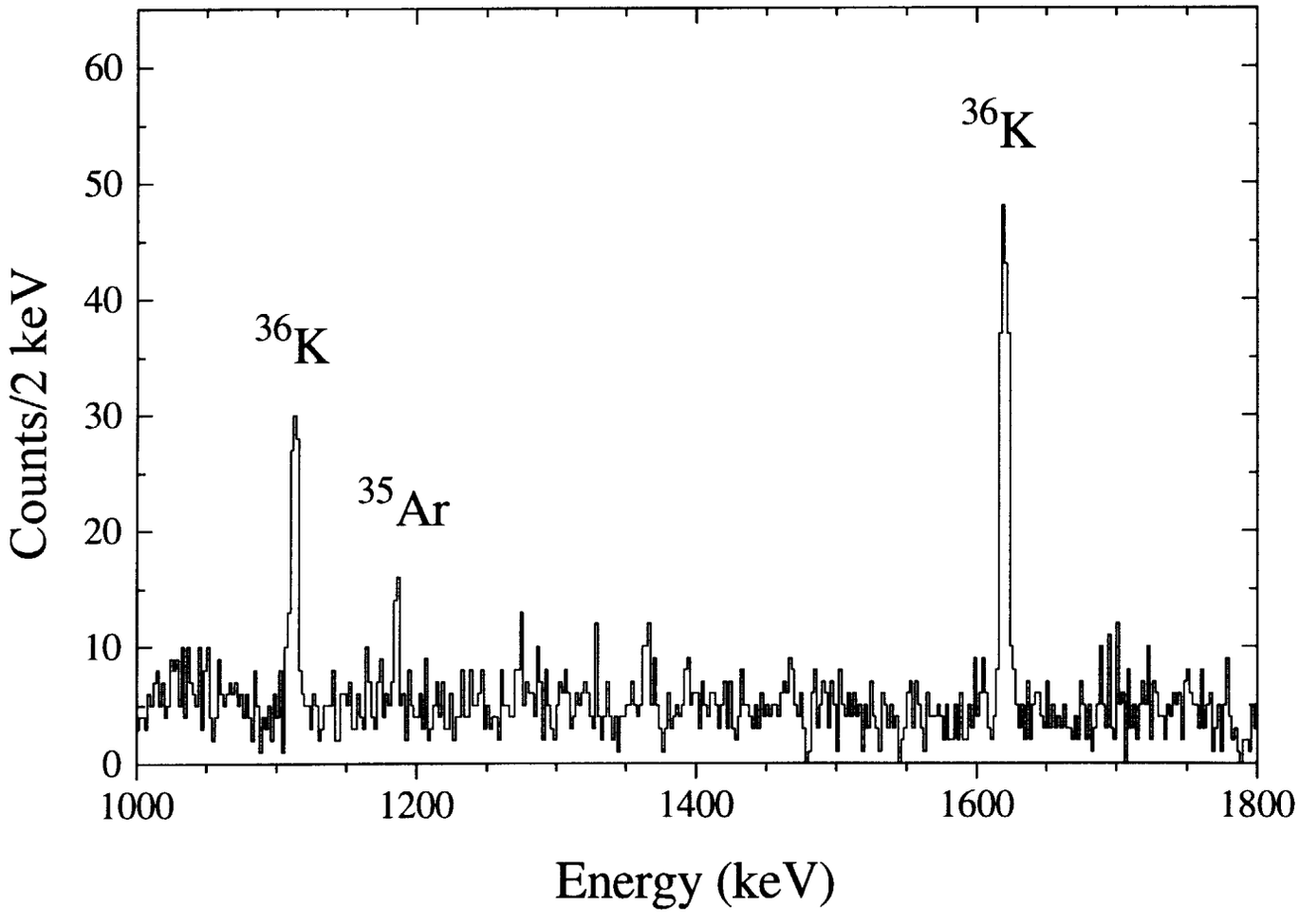
Counts/2 keV
Energy (keV)
$^{36}$K
$^{35}$Ar
$^{36}$K
0
10
20
30
40
50
60
1000
1200
1400
1600
1800

Fig. 2

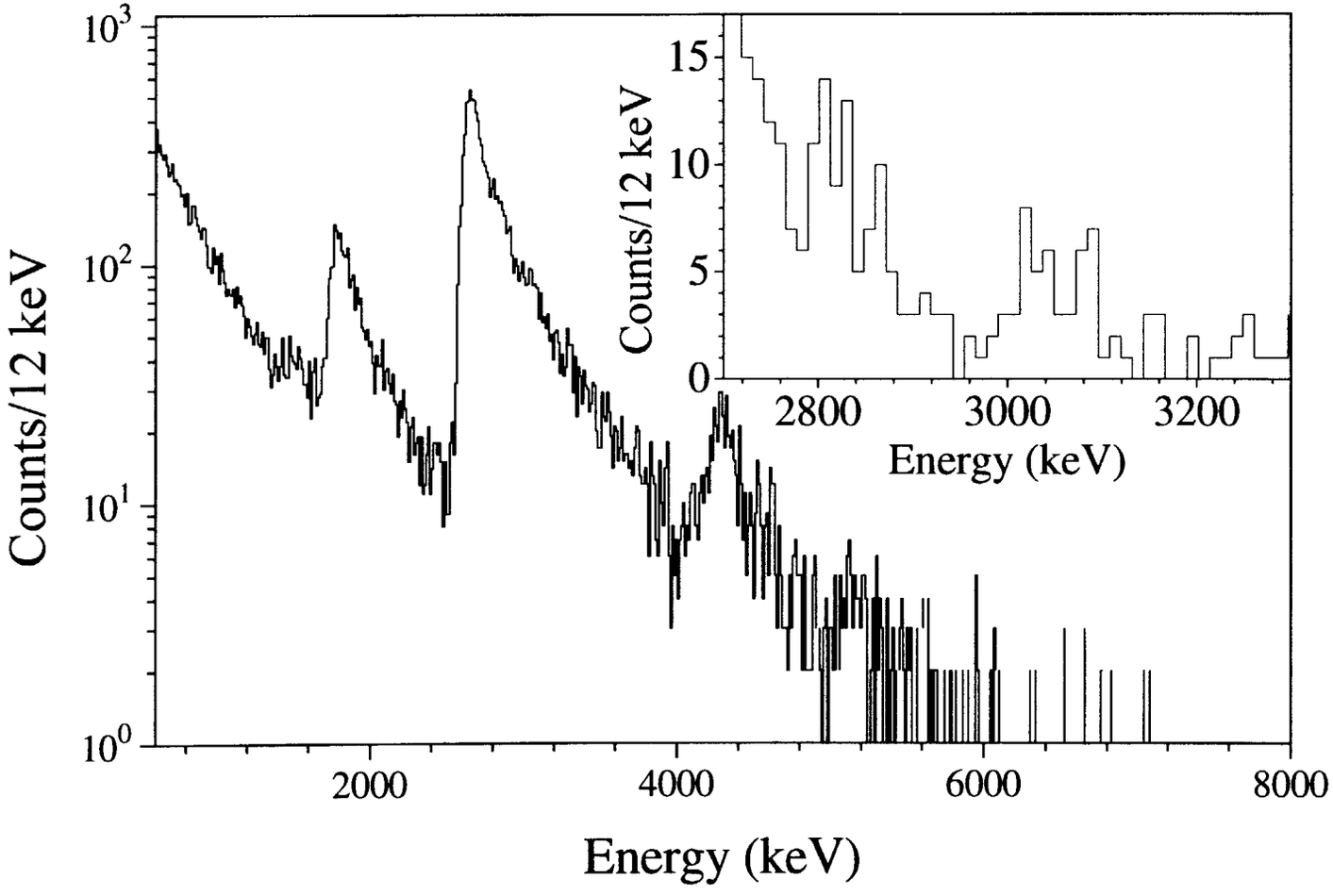
Counts/12 keV
$10^3$
$10^2$
$10^1$
$10^0$
2000
4000
6000
8000
Energy (keV)
Counts/12 keV
15
10
5
0
2800
3000
3200
Energy (keV)

Fig. 9

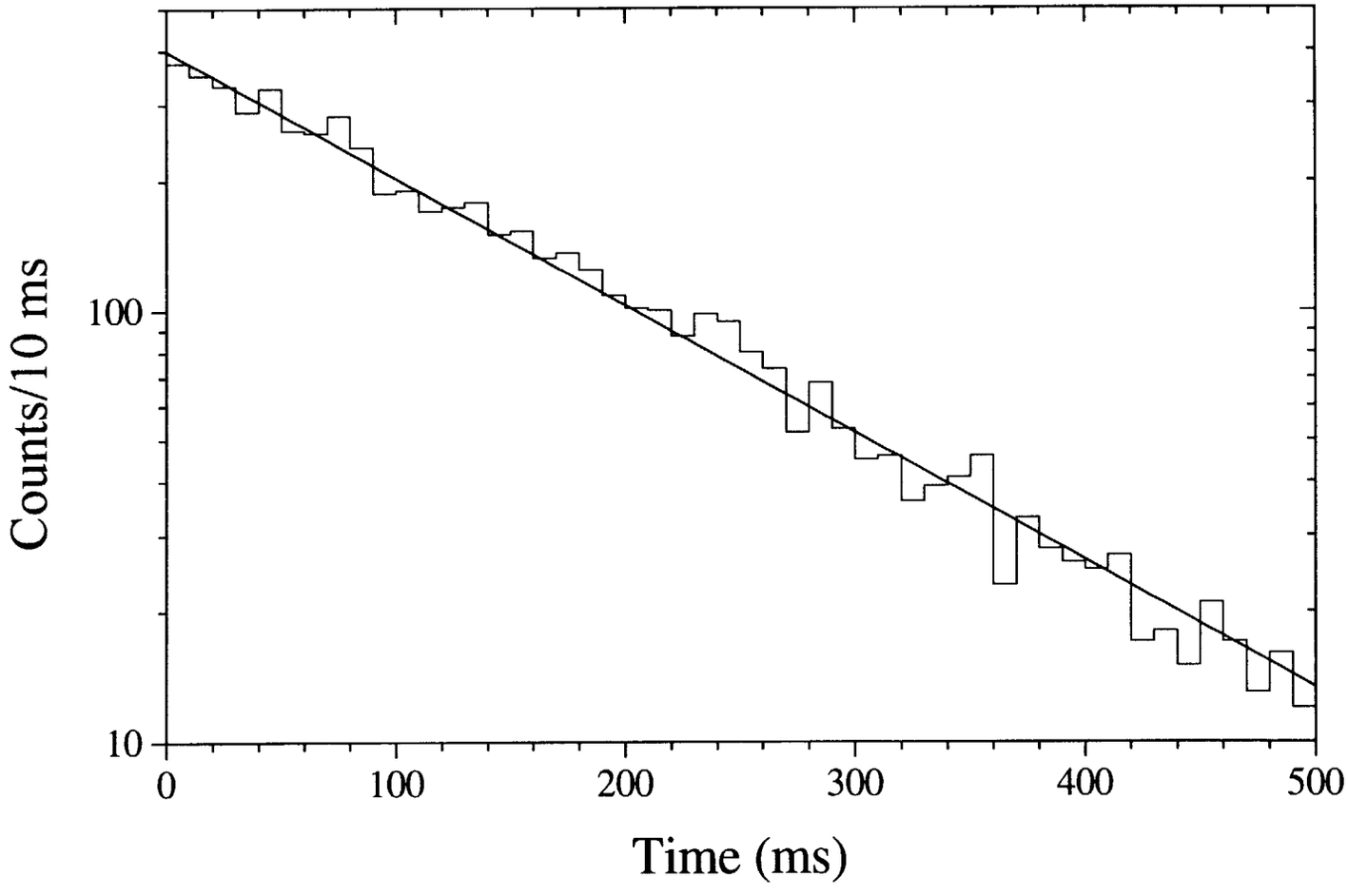


Fig. 11

Fig. 11

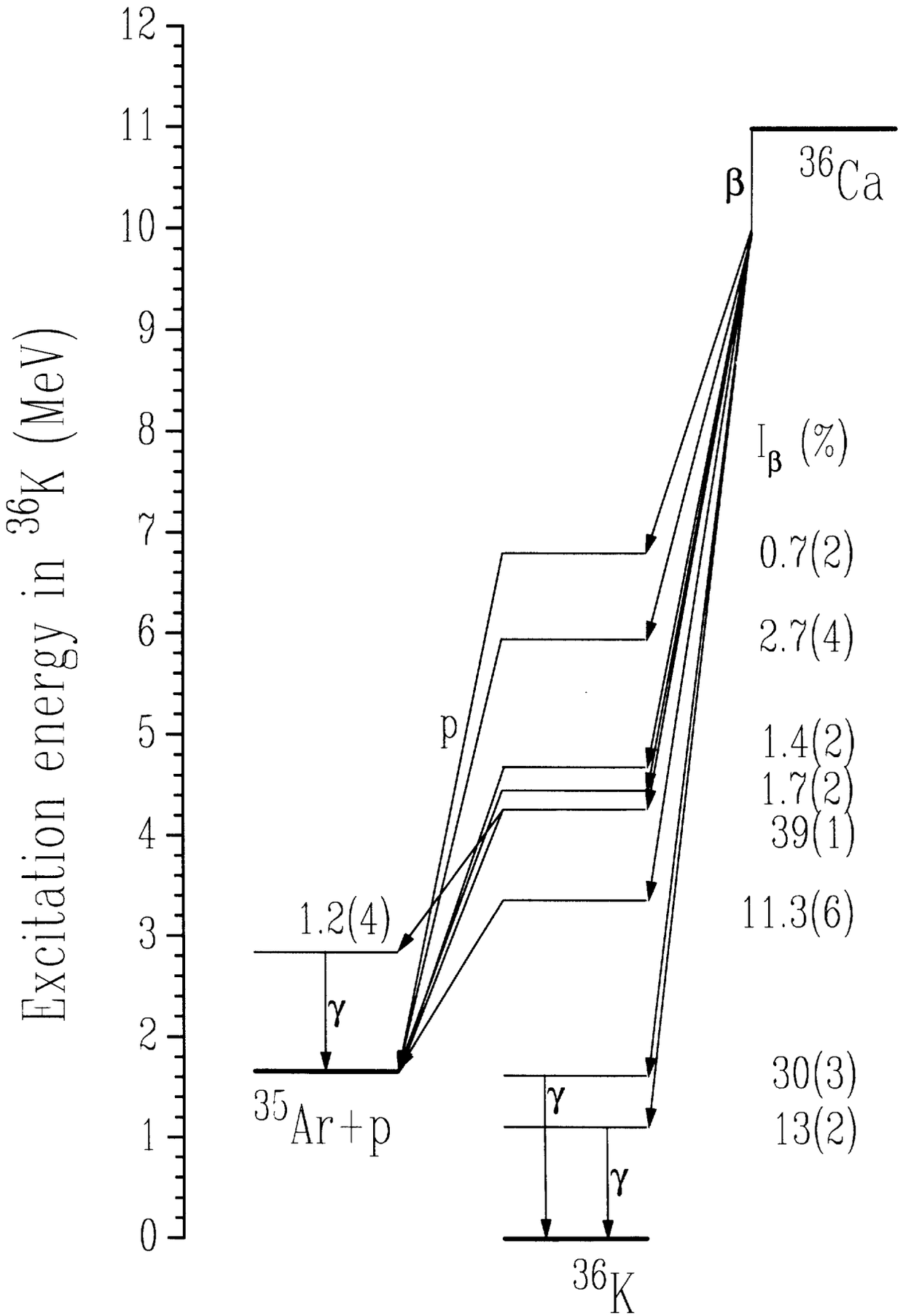
Excitation energy in $^{36}$K (MeV)
12
11
10
9
8
7
6
5
4
3
2
1
0
β
$^{36}$Ca
$I_\beta$ (%)
0.7(2)
2.7(4)
1.4(2)
1.7(2)
39(1)
11.3(6)
30(3)
13(2)
p
1.2(4)
γ
γ
γ
$^{35}$Ar+p
$^{36}$K

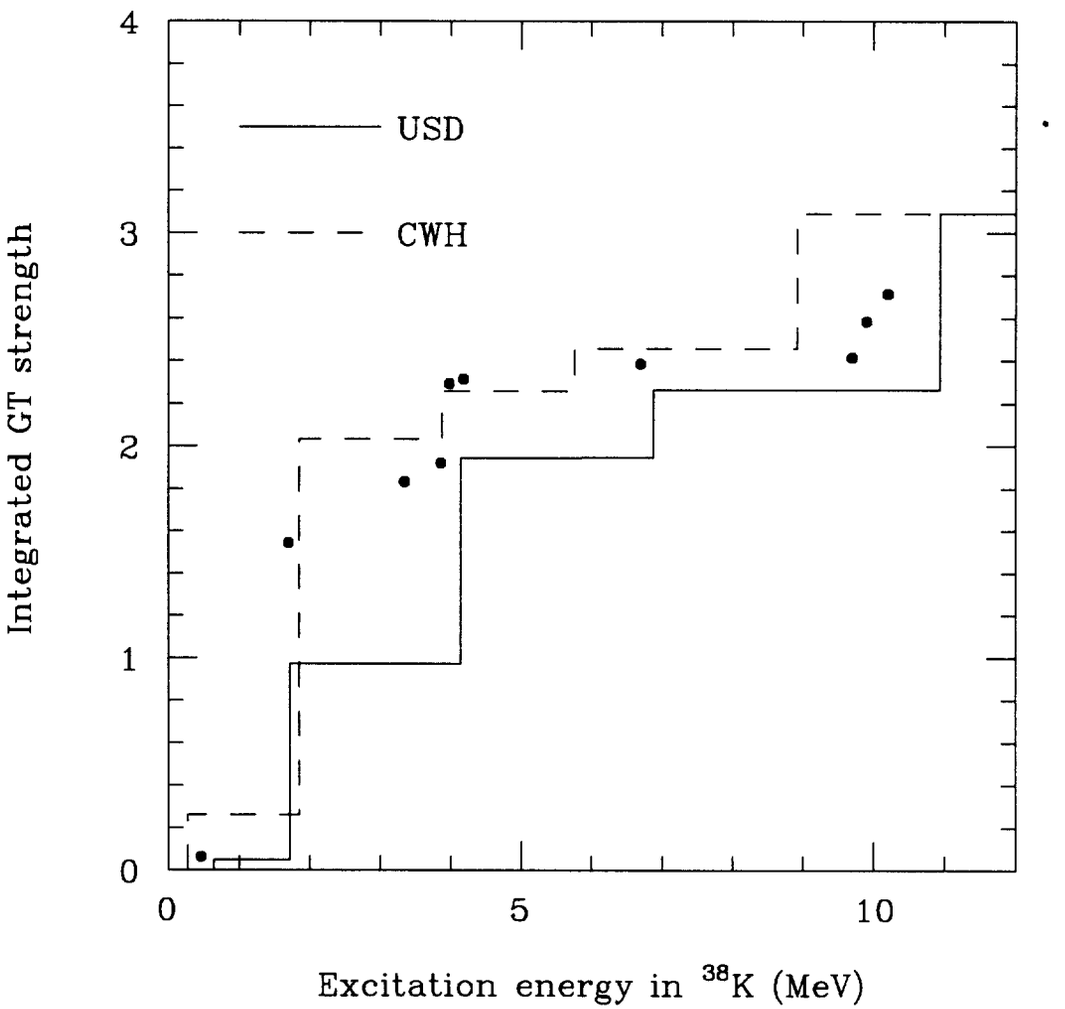
USD
CWH
Integrated GT strength
Excitation energy in $^{38}$K (MeV)
0
1
2
3
4
0
5
10

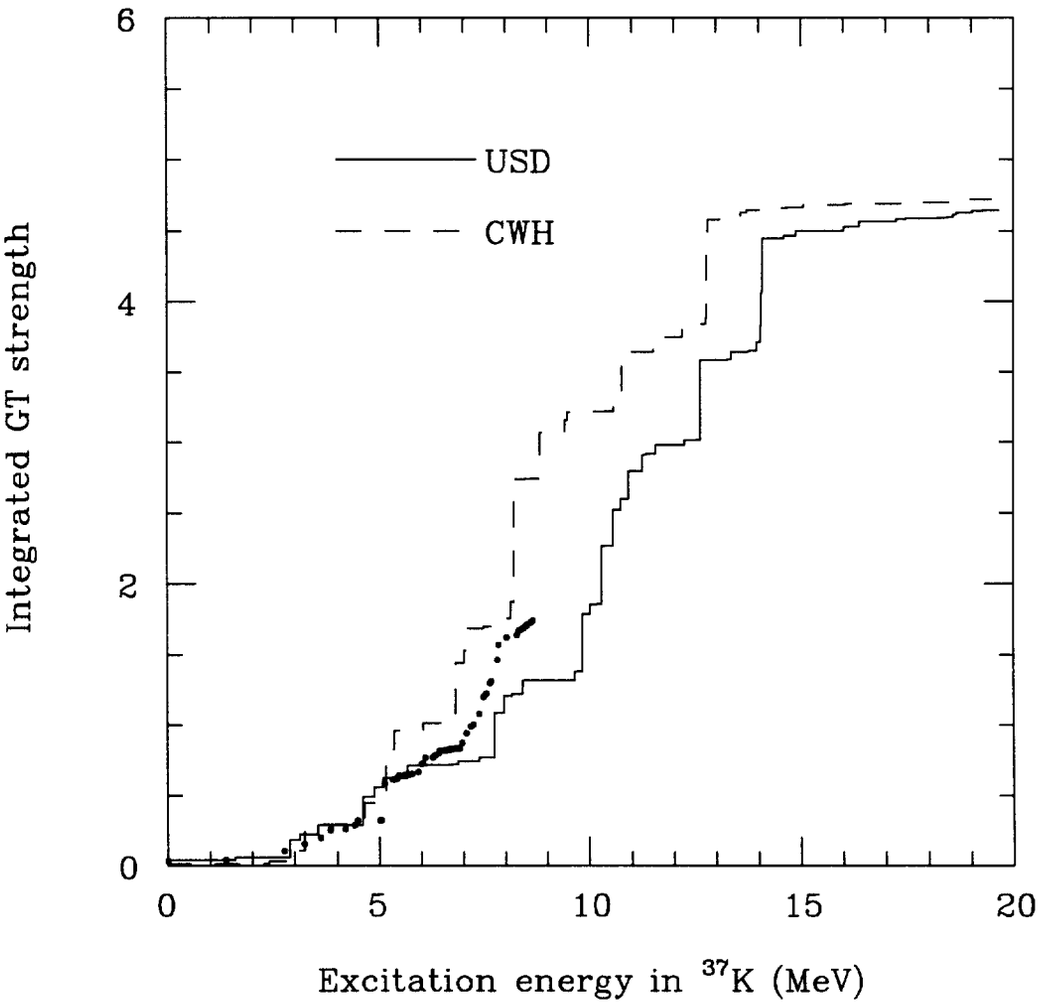
6
4
2
0
0
5
10
15
20
USD
CWH
Integrated GT strength
Excitation energy in $^{37}$K (MeV)

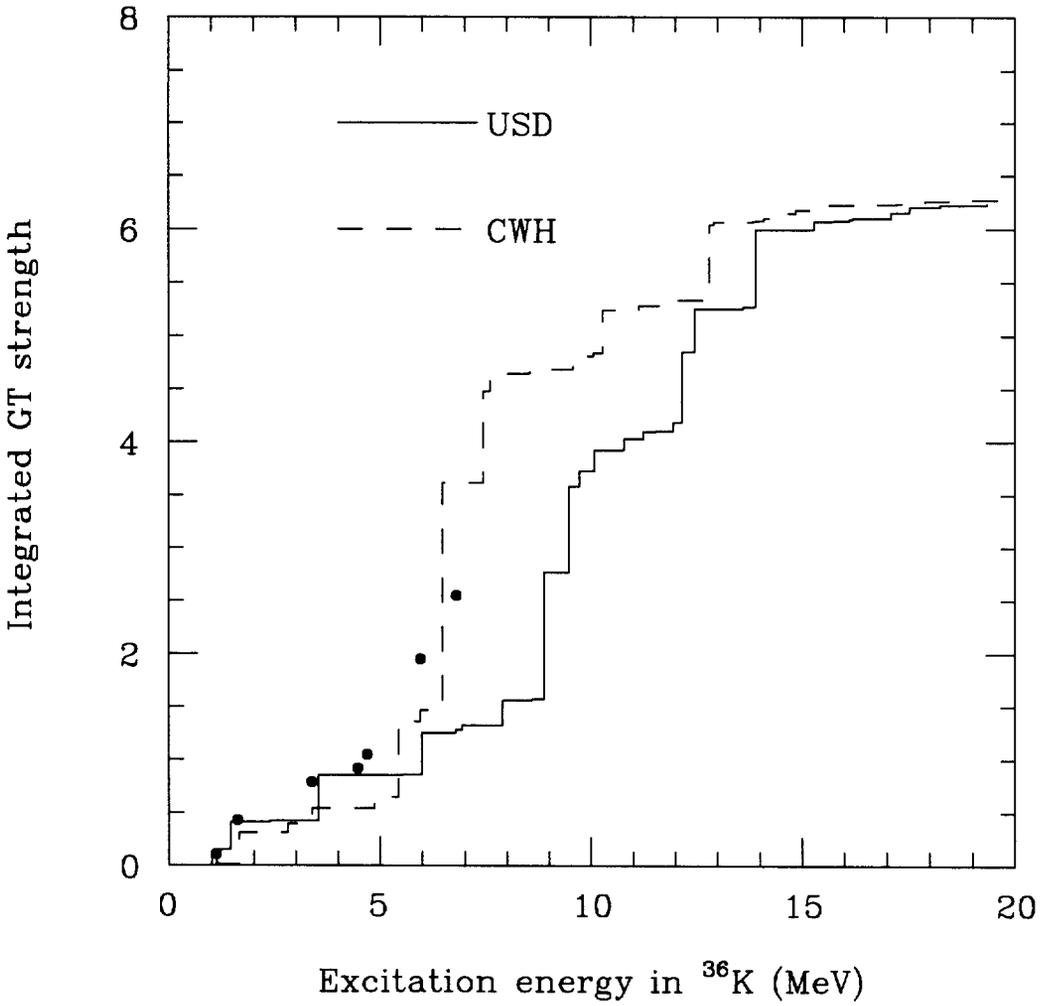
8
6
4
2
0
0
5
10
15
20
USD
CWH
Integrated GT strength
Excitation energy in $^{36}$K (MeV)

Fig. 14